2003-03-13

Channel Probing for an Indoor Wireless Communications Channel

Brandon Hunter
Brigham Young University - Provo

CHANNEL PROBING FOR AN INDOOR WIRELESS COMMUNICATIONS CHANNEL

by

Brandon Rosel Hunter

A thesis submitted to the faculty of

Brigham Young University

in partial fulfillment of the requirements for the degree of

Master of Science

Department of Electrical and Computer Engineering

Brigham Young University

August 2003

BRIGHAM YOUNG UNIVERSITY

GRADUATE COMMITTEE APPROVAL

of a thesis submitted by

Brandon Rosel Hunter

This thesis has been read by each member of the following graduate committee and by majority vote has been found to be satisfactory.

Date	Dr. Michael A. Jensen, Chair
Date	Dr. Brian D. Jeffs
Date	Dr. A. Lee Swindlehurst

BRIGHAM YOUNG UNIVERSITY

As chair of the candidate's graduate committee, I have read the thesis of Brandon Rosel Hunter in its final form and have found that (1) its format, citations, and bibliographical style are consistent and acceptable and fulfill university and department style requirements; (2) its illustrative materials including figures, tables, and charts are in place; and (3) the final manuscript is satisfactory to the graduate committee and is ready for submission to the university library.

Date

Dr. Michael A. Jensen
Chair, Graduate Committee

Accepted for the Department

Dr. A. Lee Swindlehurst
Graduate Coordinator

Accepted for the College

Douglas M. Chabries
Dean, College of Engineering and Technology

ABSTRACT

CHANNEL PROBING FOR AN INDOOR WIRELESS COMMUNICATIONS CHANNEL

Brandon Rosel Hunter

Department of Electrical and Computer Engineering

Master of Science

The statistics of the amplitude, time and angle of arrival of multipaths in an indoor environment are all necessary components of multipath models used to simulate the performance of spatial diversity in receive antenna configurations. The model presented by Saleh and Valenzuela [1], was added to by Spencer et. al. [2], and included all three of these parameters for a 7 GHz channel. A system was built to measure these multipath parameters at 2.4 GHz for multiple locations in an indoor environment. Another system was built to measure the angle of transmission for a 6 GHz channel. The addition of this parameter allows spatial diversity at the transmitter along with the receiver to be simulated. The process of going from raw measurement data to discrete arrivals and then to clustered arrivals is analyzed. Many possible errors associated with discrete arrival processing are discussed along with possible solutions. Four clustering methods are compared and their relative strengths and weaknesses are pointed out. The effects that errors in the clustering process have on parameter estimation and model performance are also simulated.

ACKNOWLEDGMENTS

Special thanks to my loving wife Laura, for her immeasurable patience and support.

Contents

List of Tables

List of Figures

Chapter 1

Introduction

Wireless communication has quickly become an important part of modern life. Cellular phones, satellites, wireless local area networks, and even broadband wireless internet services have all become readily available to most people interested in the convenience and flexibility that are the hallmarks of wireless communications. As the prevalence of these wireless products continues to expand, so does the importance of fully utilizing the capacity of communication channels. Development efforts continue to be focused on increasing reliability and speed in wireless products while minimizing the required bandwidth, power consumption, and cost.

The performance of a wireless communication system is strongly dependent on the propagation channel. When assessing this performance, it is useful to have available a statistical model that describes the channel behavior. Such models can enable the simulation and optimization of both the hardware and software systems used for wireless communication. The ability to use a model at an early stage of a design can significantly reduce the cost and time to develop wireless products.

The characteristics of an indoor environment have a drastic effect on the performance of many wireless systems. Specifically, the large number of reflecting surfaces present in an indoor channel can have a dominant effect on the necessary system complexity. Therefore, models that describe the statistical behavior of signals following multiple paths through an indoor environment are very important in helping system designers either combat or exploit the "multipath" signals.

One type of model that can be very useful represents the propagation channel using a finite set of plane waves, where the plane wave parameters are described using

statistical distributions. A model presented by other authors [2], [1], and used in this thesis (Chapter 2) accounts for spatial and temporal correlation seen in measured data by grouping the plane waves into clusters. The usefulness of such a model, however, depends ultimately on how accurately it predicts the actual statistical behavior of the channel. One approach for obtaining these statistics is to conduct experimental measurement campaigns and extract the parameters from a large ensemble of data. In this thesis two channel probing methods are described that attempt to characterize the direction of arrival (DOA), the direction of departure (DOD), the time delay, and the relative amplitude of individual multipaths in an indoor environment. Special attention is paid to the effects of clustering methods on the extraction of the channel statistics from measured data.

1.1 MIMO Systems

Multiple input multiple output (MIMO) wireless systems represent one important application where models such as those discussed in this thesis are useful. Such a system consists of multiple transmit and multiple receive antennas operating in parallel as shown in Figure 1.1. Each transmit antenna can send a unique signal while each receive antenna will receive a different combination of those signals. The MIMO approach to wireless communication is important because it can increase the channel capacity for a given bandwidth [3].

1.1.1 Environmental Effects

The capacity of a MIMO system depends on the types of antennas used, the antenna layout, and the propagation environment. In an indoor environment, the signal from each transmit antenna will generally propagate to the receiver via multiple paths through the rich scattering environment. For single input single output (SISO) systems, this propagation can lead to signal fading due to destructive addition of the multipaths. MIMO systems, on the other hand, use the multiple antennas to actually exploit the multipath propagation, generally producing increased system throughput.

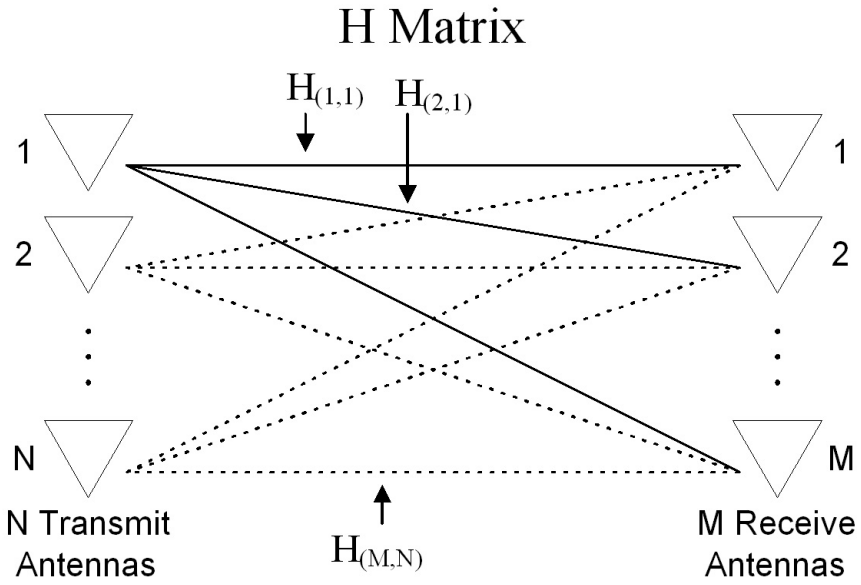

Figure 1.1: Graphical Representation of Channel Matrix (**H**)

1.1.2 Transfer Matrix

As shown in Figure 1.1, a MIMO channel with N transmit and M receive antennas can be described by a frequency and time dependent transfer function for each pair of transmit and receive antennas. These individual transfer functions can be grouped into an $M \times N$ matrix, $\mathbf{H}(\omega, \mathbf{t})$. For a narrow band signal and stationary environment, the time and frequency dependence can be neglected. The vector representing the output from the receivers is therefore $y = \mathbf{Hx} + \eta$, where $\mathbf{x}$ is the vector of transmitted signals and η represents noise. Assessing the potential performance of MIMO systems requires knowledge of this transfer matrix, either from direct measurements or from models. A large variety of channel measurements have been performed by various researchers in the field. The work of Wallace et. al. [4] in MIMO channel measurements is one such example.

In this work, we focus on using measurements of the multipath structure in a given environment to create an accurate propagation model. This model can then be used to generate the channel matrix for any given transmit and receive antenna

configuration. The channel matrices obtained from these studies can ultimately be used to determine the information carrying capacity of the channels they represent. In this work, however, we will also examine the properties of the channel itself rather than merely computing capacity. This will allow us to carefully assess the sensitivity of the constructed channel matrices to the various parameter estimation methods examined as part of the work.

1.2 Contributions of the Thesis

In this thesis several new contributions to channel modeling are presented.

1. The results of two channel probing experiments are reported. For each platform used, the following topics are covered:
   (a) Measurement Methodology
   (b) Hardware Setup
   (c) Data Processing
   (d) Measurement Results
   (e) Platform Weaknesses
   (f) Suggestions for Improved Platforms
2. Several new clustering algorithms that increase the speed, accuracy and repeatability of arrival clustering are presented, and their performance is compared.
3. The effects of clustering errors on model parameter estimation are quantified.
4. The effects of parameter errors on the statistics of model-generated channel matrices are shown:
   (a) Mean Value of Elements
   (b) Variance of Elements
   (c) Channel Capacity Estimate (Water Filling Solution)

Chapter 2

Channel Model

A model that can accurately portray the statistical behavior of a wireless channel is a valuable tool for wireless system design. Such a model allows the designer to predict the statistics of the system's performance [5] and improve the design before the first prototype is even constructed. This approach can reduce the cost and time of introducing new products. This chapter describes a model for indoor wireless propagation channels.

2.1 Saleh and Valenzuela Model

Saleh and Valenzuela measured and statistically characterized a wireless multipath channel as described in [1]. They effectively measured the "impulse" response of the channel by transmitting and receiving a sequence of narrow pulses from omnidirectional antennas. Based on these time-domain measurements, they presented a model that describes the wireless channel as the sum of discrete arrivals, each with a different delay in its arrival time. The key observation made during this research, and which has impacted many channel modeling efforts, is that these arrivals are clustered in time. The channel can therefore be described by a channel impulse response of the form

$$h(t) = \sum_{l=0}^{L} \sum_{k=0}^{K} \beta_{kl} e^{j\phi_{kl}} \delta(t - T_l - \tau_{kl}), \tag{2.1}$$

where L and K are the number of clusters and arrivals (rays) within each cluster, respectively, and T_l denotes the arrival time of the l^{th} cluster. Each multipath arrival is characterized by a delay within the cluster τ_{kl}, an amplitude β_{kl}, and phase ϕ_{kl}.

2.1.1 Time of Arrival

The absolute arrival time for each discrete signal is $T_l + \tau_{kl}$. Based upon a large volume of measurements, Saleh and Valenzuela described these arrival time parameters using statistical representations [6]. The cluster arrival time T_l is described as a Poisson random variable with arrival rate Λ. Each cluster's arrival time is conditioned on the arrival time of the prior cluster, as represented by the probability density function (PDF)

$$p(T_l|T_{l-1}) = \Lambda e^{-\Lambda(T_l - T_{l-1})}. \tag{2.2}$$

The arrival time of each ray within a cluster τ_{kl} is also described as a conditional Poisson process with arrival rate λ. This PDF is given by

$$p(\tau_{kl}|\tau_{(k-1)l}) = \lambda e^{-\lambda(\tau_{kl} - \tau_{(k-1)l})}. \tag{2.3}$$

The arrival rate λ is usually much larger than Λ, as there are typically many arrivals per cluster.

2.1.2 Phase of Arrival

The phase of each arrival is determined by the length of the path traveled, the medium through which the signal passes, and by the reflection coefficients of the scattering surfaces. The sum of these effects leads to the phase being modeled as independent of all other parameters and uniformly distributed over $[0, 2\pi)$.

2.1.3 Arrival Amplitude

The amplitudes of the clusters, as well as the rays within the clusters, decay roughly exponentially in time due to signal spreading and path loss. Mathematically, we represent the mean arrival amplitude versus time using the double exponential

$$\overline{\beta}_{kl} = \overline{\beta}_{00} e^{-\frac{T_l}{\Gamma}} e^{-\frac{\tau_{kl}}{\gamma}}, \tag{2.4}$$

where Γ and γ are the time constants for the cluster and ray amplitude decay rates respectively. The actual arrival amplitudes are then described as a Rayleigh random variable with a time-varying mean given by the double exponential.

Figure 2.1 shows one realization of this model, where the height represents the amplitude of each discrete arrival. Each cluster of the arrivals is shown in a different color.

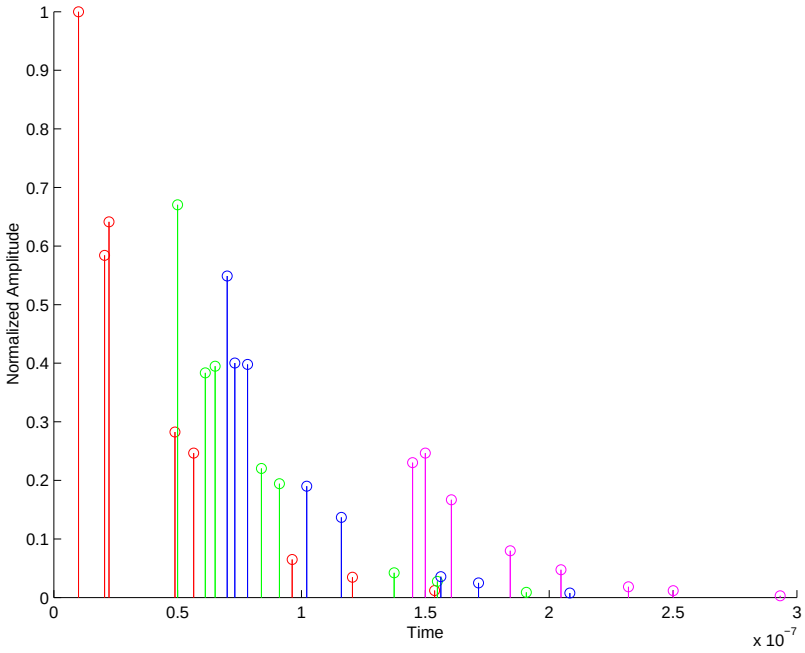

Figure 2.1: Arrival Data

In Figure 2.2 the "outer envelope" illustrates the decay profile of the cluster mean amplitudes, while the "cluster envelope" illustrates the ray mean amplitudes within each cluster. Figure 2.3 shows how actual arrivals line up along the mean amplitude envelopes.

2.2 Model Modifications

Spencer et. al. [2] extended the Saleh Valenzuela model to include azimuth angle of arrival information. This is necessary for simulating realistic responses for multiple antenna systems. The angle of arrival information can be used to recombine all of the discrete arrivals with the correct phase adjustment at each different antenna

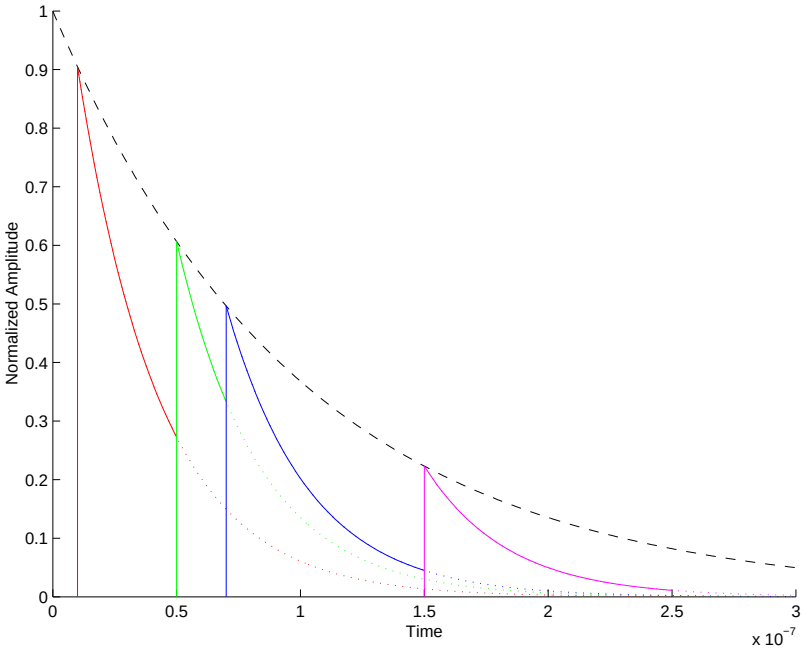

Figure 2.2: Cluster and Arrival Amplitude Decay Envelopes

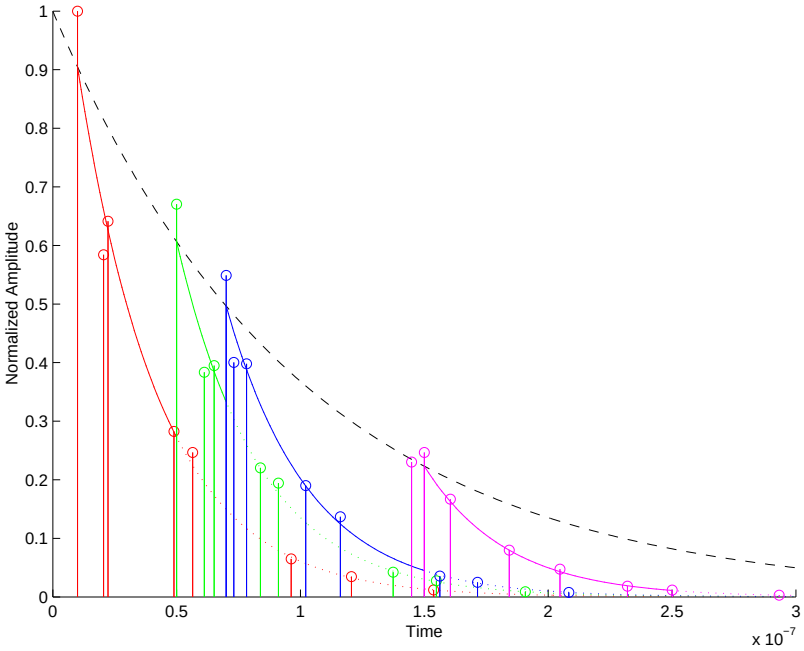

Figure 2.3: Arrivals Superimposed on Envelopes

position. To measure the "impulse" response of a wireless channel with azimuth angle of arrival information, Spencer used a network analyzer to measure the time-domain response of a wireless channel using an omni-directional transmit antenna and a rotating directional receive antenna for incoming arrival spatial resolution.

2.2.1 Angle of Arrival

According to the extended model the temporally grouped clusters, as described by Saleh and Valenzuela, are clustered in arrival angle as well. The cluster angles, or the mean value of the angles of arrival in each cluster, are taken to be independent from each other and distributed uniformly over 360°. The arrival angles within each cluster, θ, are modeled as Laplacian random variables with variance σ^2 centered at the angle Θ_l:

$$p(\theta) = \frac{1}{\sqrt{2}\sigma} e^{-|\frac{\sqrt{2}(\theta-\Theta_l)}{\sigma}|}, \tag{2.5}$$

When the cluster angles Θ_l, and the ray angles θ_{kl} are included, the extended impulse response can be represented by

$$h(t,\Theta) = \sum_{l=0}^{L}\sum_{k=0}^{K} \beta_{kl} e^{j\phi_{kl}} \delta(t - T_l - \tau_{kl})\delta(\theta - \Theta_l - \theta_{kl}). \tag{2.6}$$

The inclusion of the angle of arrival in the model makes it possible to determine the spatial variation of the field. Such information is necessary in assessing the performance of MIMO and other systems utilizing multiple antennas [7].

2.2.2 Point Spread Function

In the system impulse response given by Equation (2.6), the delta functions are used to indicate that the arrivals are from point sources or point reflections in accordance with a specular model. However, the measurement system used to extract the values of the underlying parameters has limited resolution in time as well as in angle, resulting in blurring of the signal in time and space. The true direction and time of the arrivals are determined by deconvolving the Point Spread Function (PSF) of the measurement system from the measured raw data [8]. The temporal spread

of the PSF is determined by the bandwidth and windowing used in the time-domain measurement apparatus. The angular spread is determined by the antenna pattern of the receiving antenna. In Spencer's work, this PSF was measured in a quasi multipath-free environment, and the deconvolution was performed using the CLEAN algorithm [9].

Chapter 3

Channel Probing

Two channel probing experiments are performed to measure and statistically characterize the multipath characteristics of an indoor environment. The first experiment measures the angles and times of arrival for multipath returns at 2.4 GHz in an indoor environment. The second experiment measures the angle of departure and the angle of arrival for multipath signals at 6 GHz in the same environment. The results of both of these experiments are used to more fully understand the characteristics of multipath in an indoor environment [10], [11]. They are also compared to the results reported by Saleh and Valenzuela [1] and Spencer et. al. [2].

3.1 A 2.4 GHz System

The 2.4 GHz system is similar to the platform used by Spencer for the measurements in [2], with a few modifications. There are several reasons for conducting this new measurement campaign. First, the new system operates at a center frequency of 2.4 GHz, which is a commonly used frequency for indoor communication, compared to the 7 GHz measurements that Spencer performed. Second, the new system has several performance enhancements, including improved angular resolution, communication range, and dynamic range. The system uses an omni-directional transmit antenna and a directional receive antenna on an antenna positioner. A single data set consists of measuring the temporal impulse response between two locations for 180 angular orientations of the receive antenna. Between each successive measurement, the receive antenna is rotated 2°. During each impulse response measurement, both antennas are kept stationary. All 180 measurements are then combined to form the

unique temporal and spatial impulse response for that particular pair of antenna locations. The impulse responses from all location pairs are processed and then used to estimate the parameters for the modified Saleh and Valenzuela model. One significant weakness in this approach is that it relies on time invariance for the duration of the measurements. A typical measurement can take up to 30 minutes, so it is likely that some errors due to time variance appear in the measurements.

3.1.1 Measurement Methodology

Rather than develop or purchase a narrow pulse source and a high bandwidth receiver to measure the multipaths, a frequency-domain solution is implemented. An HP8720B network analyzer is used as a source and swept from 2.1 to 2.7 GHz. The HP8720B measures the received signal, $\mathbf{b_2}$, and divides it by an internal reference channel measurement, $\mathbf{a_1}$. This comparison, $\frac{\mathbf{b_2}}{\mathbf{a_1}}$, is a standard network analysis measurement commonly known as the S_{21} frequency response. The complex frequency-domain data is subsequently transformed into a time-domain impulse response. To accomplish this the network analyzer windows the frequency-domain data and then performs a discrete Fourier transform on the results. The effective measurement is that of a band-limited impulse response. With the assumption that the channel is a linear, time invariant system, the results of this process are the same as if an actual pulse were transmitted and received.

For the impulse response, as obtained by the frequency to time-domain transformation, the temporal resolution (Δt) is determined by the frequency range (BW) according to the relationship

$$\Delta t = \frac{1}{BW}. \tag{3.1}$$

The .6 GHz bandwidth (BW) that is used for these measurements results in a temporal resolution of approximately 1.67 ns, which corresponds to a distance of .5 meters in free space. Therefore, the system is able to resolve multipath arrivals that occur at the same angle, if they occur more than 1.67 ns apart.

The finite number of samples taken in the frequency-domain measurement limit the total range of time (T_{Range}) over which valid signals can be measured. The range is given by the relationship

$$T_{Range} = \frac{1}{\Delta f}, \tag{3.2}$$

where Δf is the spacing between the frequency samples. Any signal with a delay longer than T_{Range} will be aliased in the time-domain and distort the measurement. To ensure that this does not happen in these measurements, $\Delta f = 1MHz$ is used for the frequency-domain samples. This allows 1 μs for the signals to return, which is ample time for the exponentially decaying signal to drop below the system noise floor.

3.1.2 Hardware Setup

The hardware setup for this measurement is shown in Figure 3.1. Port 1 of the network analyzer is used to step through 601 frequency points from 2.1 to 2.7 GHz. This signal is immediately amplified and sent through up to 500 feet of cable and again amplified for transmission. A quarter-wave monopole antenna on a ground plane is used to transmit the signal which is received by a dish antenna with a broadband feed [12]. The receiving antenna is mounted on an antenna positioner with 360° horizontal rotation capabilities. The signal from the antenna is amplified by a low-noise amplifier, and then received by port 2 of the HP8720B network analyzer. Typically both antennas are kept motionless for one measurement, the signal is transmitted and received, and then the receiver is rotated 2°. This is repeated until the dish has rotated a complete revolution.

The receive antenna is an ellipsoidal antenna, 90 cm. in diameter, illuminated by a broadband feed. At 2.4 GHz the beamwidth is approximately 9°. The broadband feed illuminates the antenna dish differently as the frequency changes, resulting in a frequency dependent effective aperture. This, in conjunction with the ellipsoidal dish shape, make it such that the antenna beamwidth remains fairly constant over the entire bandwidth. For most measurements the transmitter and receiver are separated

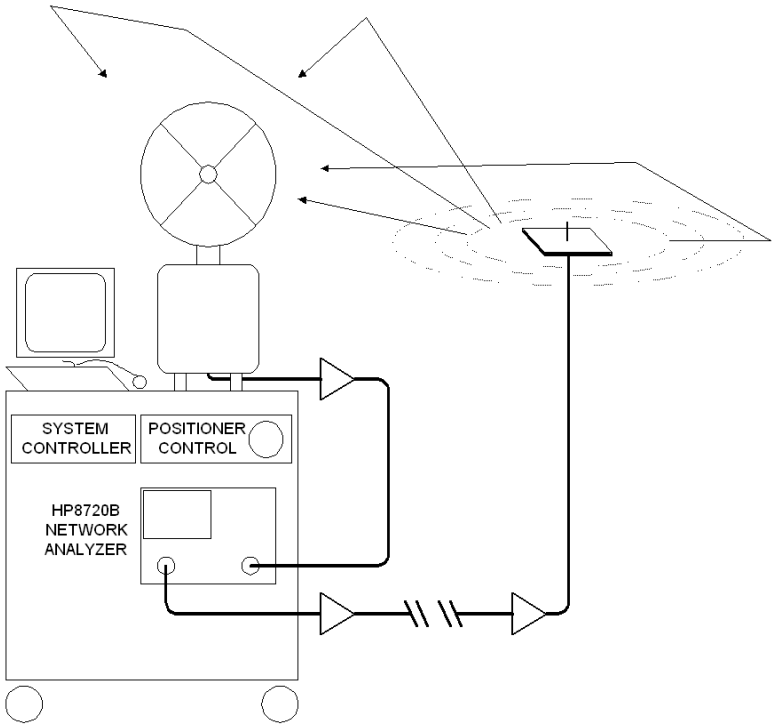

Figure 3.1: 2.4 GHz System

enough to be in the far field. However, many reflecting surfaces are in the near field of both antennas. The resultant nearfield interactions are not examined as a part of this work.

As explained in Section 2.2.2, the system response blurs the actual channel response. To remove the effects of this blurring, the two-dimensional PSF of the system is measured at an antenna range on the roof of the Clyde Building. By taking the channel impulse response in a location with minimal reflecting surfaces, the antenna pattern combined with the temporal pulse shape is determined. The resulting image provides the shape in angle and time of a single return, or, the PSF, as shown in Figures 3.2 and 3.3. To make sure that only the effects of the system end up in the PSF, the measurement is temporally gated. This removes the reflection from the ground, as well as reflections from any objects around the antenna range.

The accuracy of the PSF is very important for subsequent data processing. The amplitude, angle, and time for each arrival are determined by deconvolving the

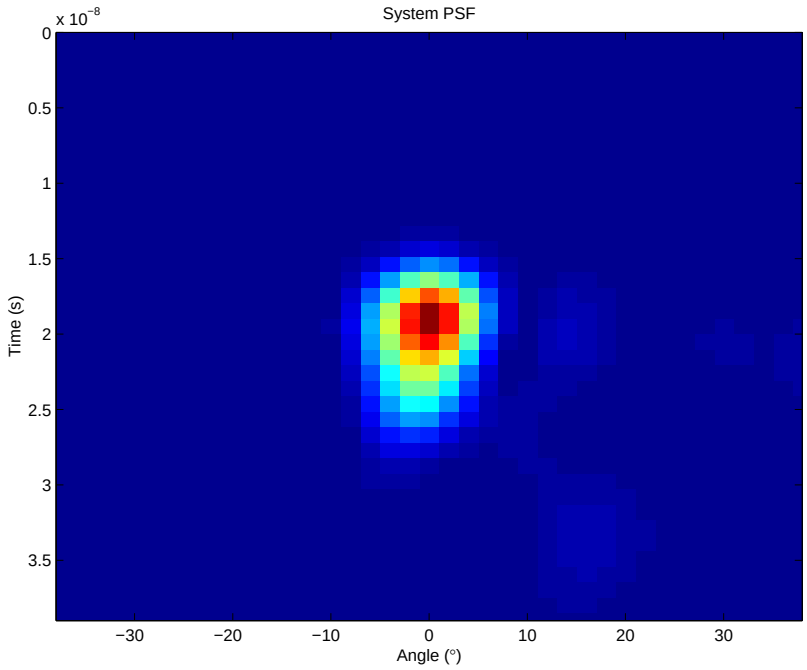

Figure 3.2: PSF Image

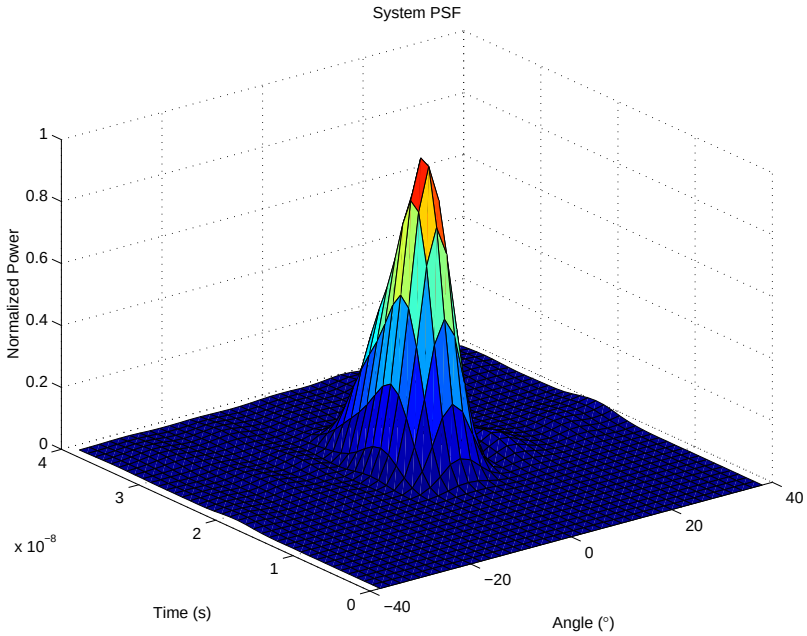

Figure 3.3: PSF Surface

PSF from the raw data. Errors in the PSF can cause inaccurate amplitudes, times, and angles being applied to the arrivals, as well as both false and missing arrivals.

3.1.3 Data Processing

The 2.4 GHz system measurement data can be used to create an image that represents the amplitude received as a function of angle and time. According to the model, this image is the two-dimensional convolution of the system PSF (Figure 3.2) with the system impulse response (Equation (2.6)). The angle, time, and amplitude of the discrete returns can be estimated from this data. These measurement results are processed in much the same manner as described by Spencer et. al. [2]. A deconvolution of the PSF from each image is performed according to the CLEAN algorithm [9] with the addition of constant-false-alarm-rate (CFAR) detection [2]. This is done by assuming that the point with the highest amplitude on the image represents a single return. The angle, time, and amplitude of this arrival are stored, and the PSF, scaled by the determined amplitude, is subtracted from the data. The highest point in the remaining data is the next arrival. This successive subtraction of each arrival from the image continues until a predetermined threshold is reached. This threshold is not fixed across the image, but rather is set by the average signal strength in the surrounding area. After all arrivals are processed, the resulting data is grouped into clusters in angle and time. Figure 3.4 shows an image with multiple arrivals generated using the PSF shown in Figures 3.2 and 3.3. The estimated arrival locations are shown in Figure 3.5 as symbols on the image.

The clustering process is described more fully in Chapter 4. In general the clustering consists of viewing the discrete arrivals plotted versus angle and time, and selecting those that appear to be clustered together based on any combination of angle, time, or amplitude values. Using an image as shown in Figure 3.4, this can be performed relatively easily by hand for widely spaced cluster centers with tightly spaced arrivals. Overlapping clusters, widely spread arrivals, or even densely populated images can all create difficulties for this manual clustering approach, leading to errors in model parameter extraction as well as poor repeatability and consistency in

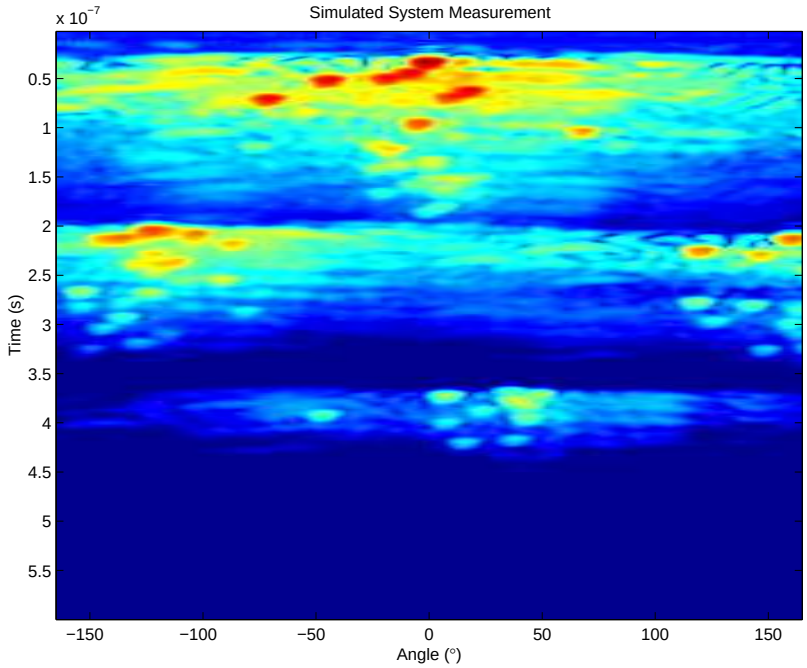

Figure 3.4: Simulated System Measurement Image

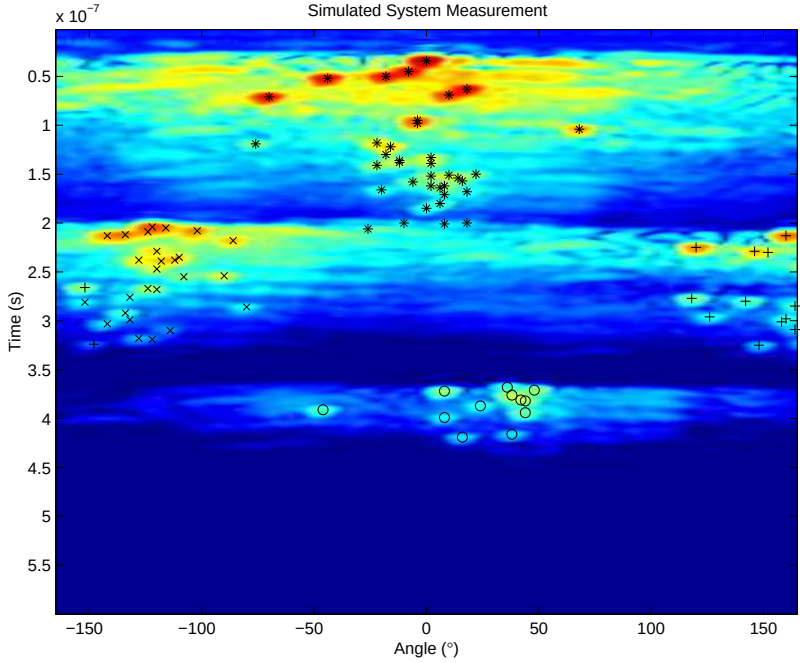

Figure 3.5: Arrivals Points on Simulated Image

data processing. Several clustering methods and their relative strengths and weaknesses are discussed in Chapter 4. Figure 3.6 shows one possible clustering for the data shown in Figures 3.4 and 3.5.

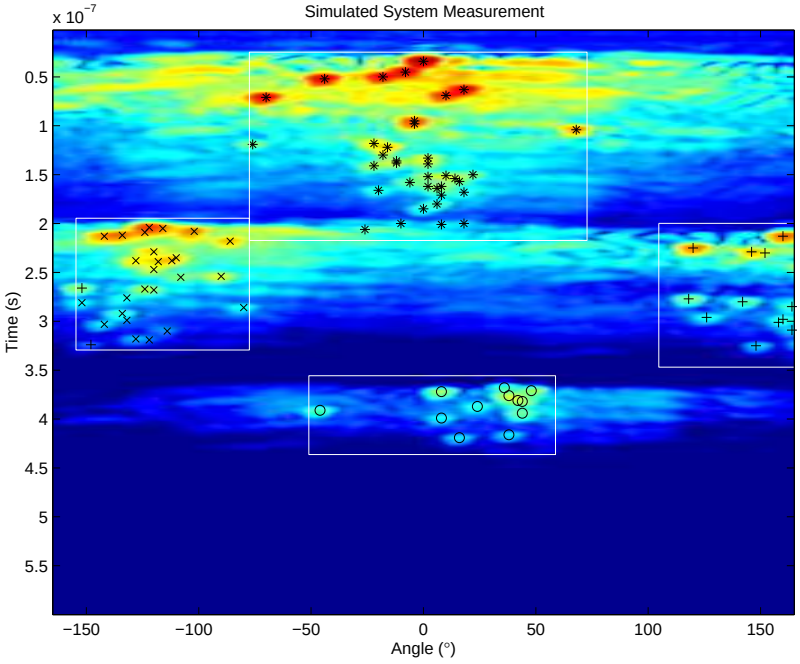

Figure 3.6: Clustered Arrivals on Simulated Image

3.1.4 Measurement Results

Over a hundred data sets were taken with the 2.4 GHz system at different locations within the Clyde Building at Brigham Young University. Figures 3.7 and 3.8 show two of these measurements. The high density of signal power made it very difficult to accurately deconvolve the arrivals. These data sets were processed using the CLEAN algorithm without CFA detection. A minumum threshold was set for arrival amplitudes to limit the processing time. Figures 3.9 and 3.10 were deconvolved using this flat threshold. At the peak of both images, the arrivals are much too dense for accurate deconvolution. While in Figure 3.10 it is obvious that

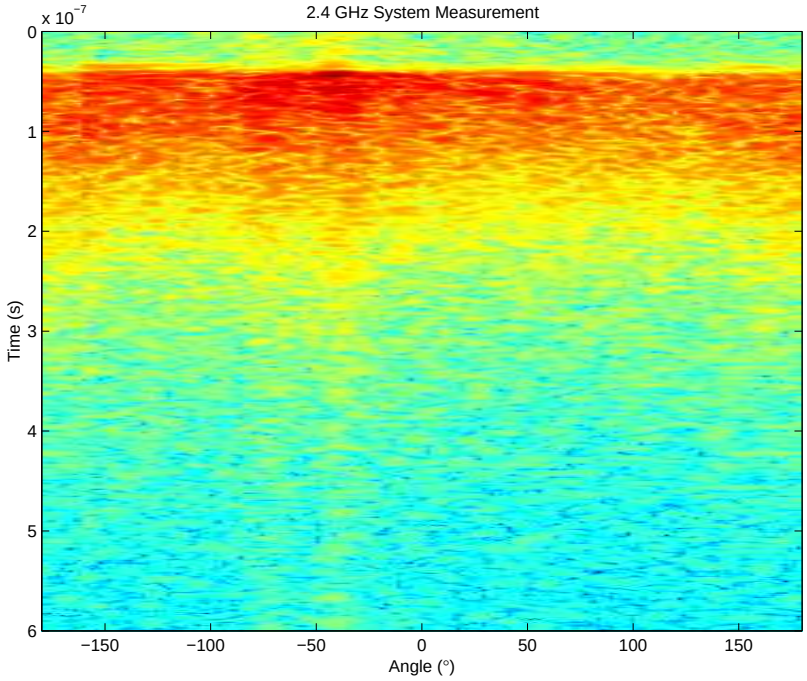

Figure 3.7: 2.4 GHz System Measurement A

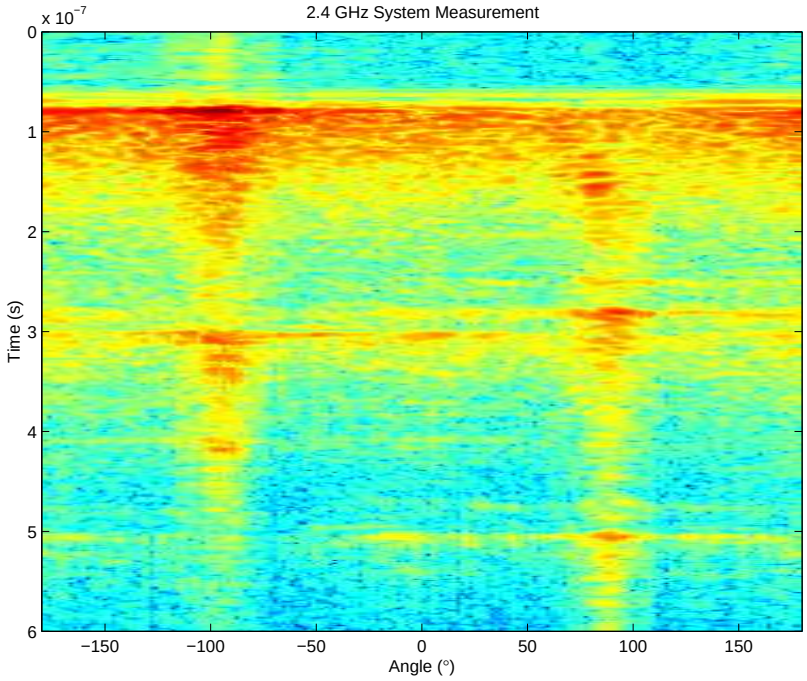

Figure 3.8: 2.4 GHz System Measurement B

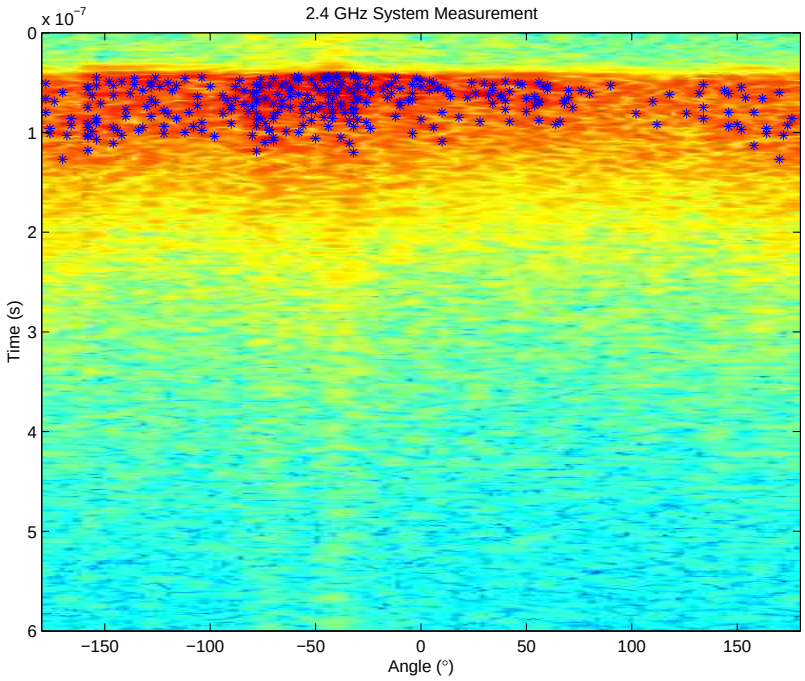

Figure 3.9: Measurement A with Arrivals

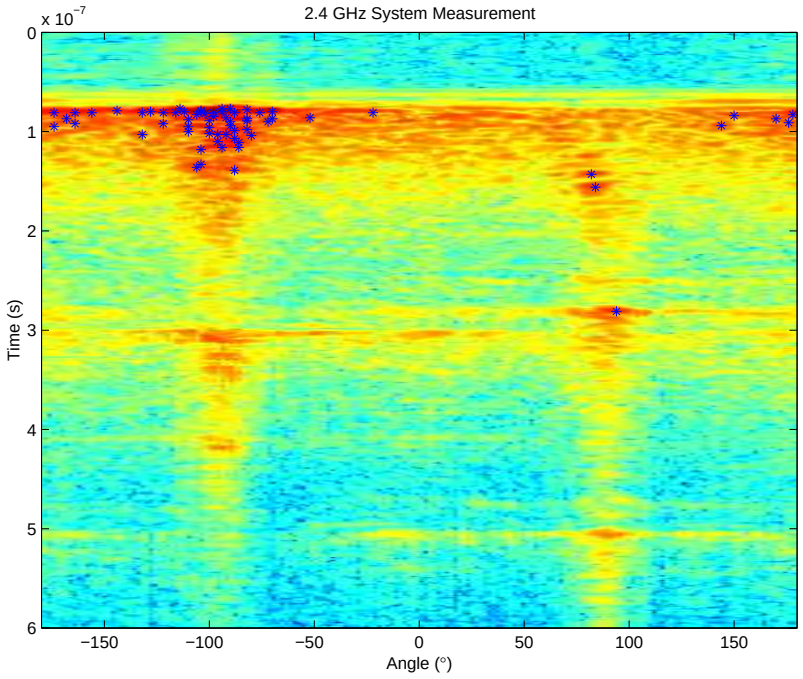

Figure 3.10: Measurement B with Arrivals

several arrivals have gone undetected due to the flat threshold. Using CFA detection would reduce the arivals in the dense areas and pick up the isolated returns, but the lost arrivals in the dense areas are actually stronger than the isolated returns. Either approach introduces problems with the deconvolution results.

The key qualitative difference between the results from this 2.4 GHz platform and those from the 7 GHz system used by Spencer were a significantly increased number of arrivals. This can partially be attributed to 2.4 GHz system's narrower antenna beamwidth, lower frequency range, and higher signal to noise ratio. There is also less path loss for this lower band. However, during this data analysis, several problems in the overall processing framework became evident. These findings impact the accuracy of the results from the data processed here as well as that processed by Spencer.

PSF Measurement Error

The PSF for this system was measured multiple times and found to be only partially repeatable. For example, the amplitude of the main sidelobes of the antenna pattern varied about 5 dB from one measurement to the next. Figure 3.11 shows the antenna pattern extracted from several PSF measurements that were taken on the Clyde Building antenna range. There are several possible explanations for this lack of repeatability. Any changes in the environment over time either during one sweep, or between sweeps, will contribute to the variation seen in the measurements. The measurement uncertainty due to the instrumentation could also have a significant affect on the results. The network analyzer, amplifiers, and cables all change their responses with temperature and due to mechanical shifting or vibrating. All of these effects contribute to the total uncertainty in the measurement.

Figure 3.12 shows the temporal pattern extracted from the same PSF measurements. The shape changes near the peaks of both patterns are the most problematic, as this PSF uncertainty causes significant difficulties in processing the measurements. It becomes impossible to determine if a signal more than 13 dB below the largest arrival is a separate arrival, or just an artifact of the measurement variability. This

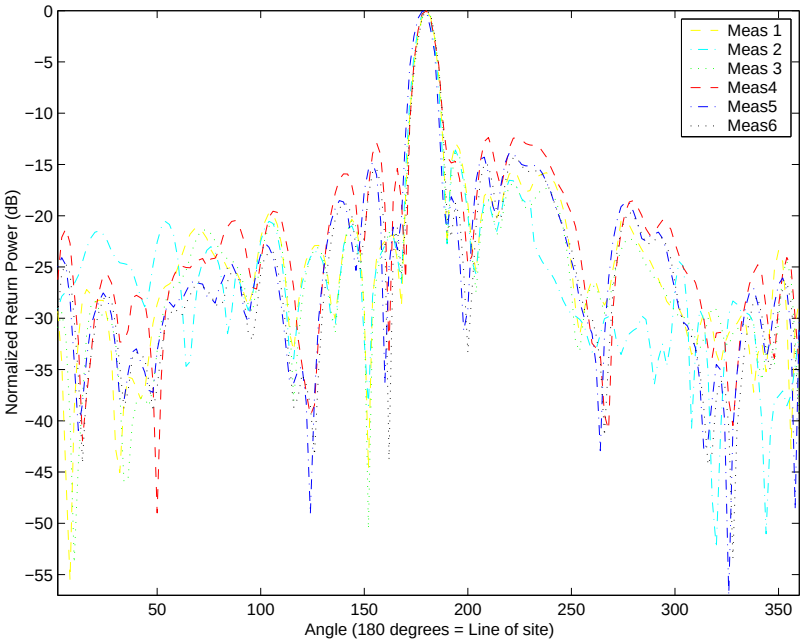

Figure 3.11: Repeated Measurements of Antenna Pattern

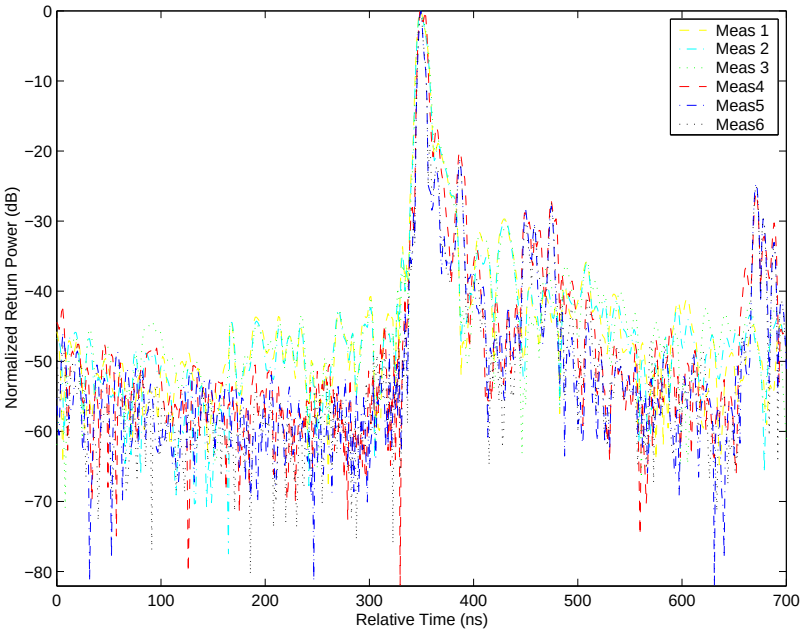

Figure 3.12: Repeated Measurements of Temporal Pattern

is in spite of the fact that the actual system noise floor is 50 dB below a typical line-of-sight measurement.

Without a more repeatable PSF measurement, the simplest solution is to discard any arrivals that are more than 13 dB below the highest data point. Figures 3.9 and 3.10 show how arrival processing is affected when a flat threshold is used. To estimate how significantly this affects our results the percentage of power below the -13 dB threshold and above the noise floor is calculated. While the percentage for each data set varies significantly with the dynamic range and the density of arrivals, on average 35% of the signal power in each data set is below the -13 dB threshold. Any arrival information processed out of this measurement subset is considerably less valuable in forming the statistical models discussed in this work.

Magnitude-Only PSF Estimate

Even with a perfectly stable PSF measurement, the algorithm used above has other flaws. The CLEAN algorithm relies on the ability to measure the strongest arrival, remove it from the image, and then move on to the next arrival. The PSF of this system is measured without phase information. Since the sidelobes of one arrival may have destructively or constructively interfered with another arrival, the phase information is crucial to being able to remove the first arrival without erasing the second arrival. The effects of the phase errors type of processing error are nearly identical to having an unrepeatable PSF measurement as described above. In both cases the any signal at or below the first sidelobes can be unique arrivals or artifacts of the larger arrivals. Again to avoid these errors, an artificial threshold can be set, allowing only the strongest returns to be processed. An estimate of the percentage of the signal power below an arbitrary threshold can be obtained from the Cumulative Distribution Function (CDF) for these measurements (Figure 3.13).

The phase information is also necessary to remove errors due to not rotating about the phase center of the antenna (Section 3.2.2). If rotaton axis for the mounted antenna does not exaclty coincide with the phase center, then the signal received at each angle represents the signal for a different point in space. This invalidates one

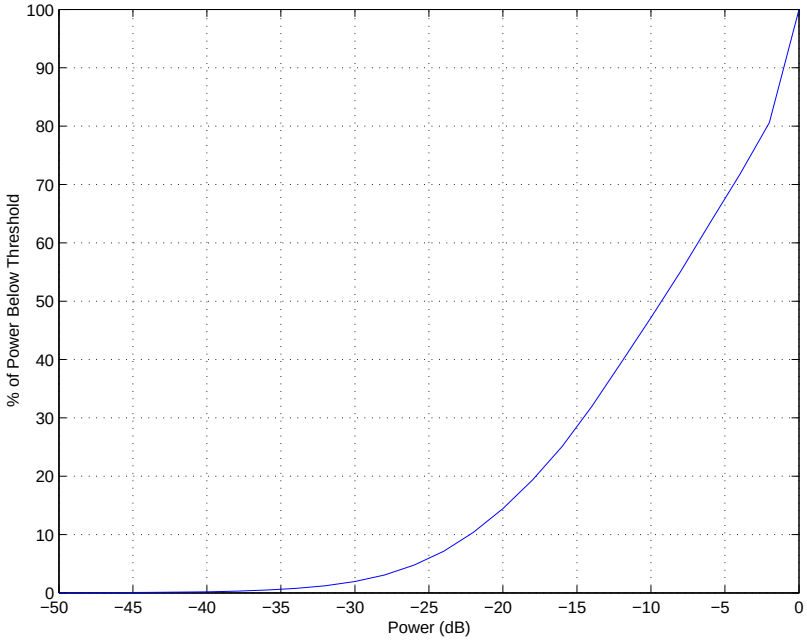

Figure 3.13: Signal Power CDF

of the initial assumptions, which is that the signals received at each angle, when combined, represent the signal that would be received at a single point. Measuring the phase, and using it for deconvolution allows for some error in mounting the antenna.

Constant False Alarm Detection

The high density of arrivals in the measurements, results in signal dependent clutter surrounding the strongest arrivals. This clutter is not due to noise sources, but rather due to valid arrivals whose position in angle and time place them near stronger arrivals. The CFA detection approach uses the average power of the area surrounding an arrival to determine a minimum threshold for arrivals. The CFA detection stops the CLEAN algorithm from processing the signal dependent clutter surrounding each large return. At the same time the CFA detection allows the CLEAN algorithm to process weaker arrivals that happen to be isolated from strong returns. While the CFA detection only weeds out smaller arrivals if they are in the vicinity of larger

ones valid arrival data still gets rejected. Also, having weak arrivals in some areas and not in others is problematic as well. Any statistics gathered using this approach must be suspect. Rather than processing some weak arrivals and rejecting others it is reasonable to simply disable the CFA detection, and apply a flat threshold across the data set. The amount of signal power lost in this approach can be estimated using Figure 3.13.

Conclusions from 2.4 GHz System

Each of the problems listed above can be avoided if the dynamic range of the system is artificially lowered. By only accepting the strongest arrivals, the dominant characteristics of a channel are captured, without processing false arrivals. From these arrivals the parameters of the system can be estimated with the realization that a significant number of arrivals are left out. As a result of these processing issues the data obtained was not used to estimate the parameters for the modified Saleh and Valenzuela model. Despite this fact the measurement campaign was useful in that the raw data can be used to create "measured" channels for MIMO system simulations.

Even without "perfect" arrival processing, the raw data indicate that the system is measuring many more arrivals than measured by Saleh and Valenzuela or by Spencer et. al. As indicated above, this leads to arrival processing problems, as well as clustering errors. Several clustering methods and their relative strengths and weaknesses are discussed in Chapter 4. These clustering methods apply both to this data as well as to the data gathered by Spencer.

The problems caused by the PSF uncertainty are also present in the data collected by Spencer et. al. Their system PSF was measured inside of a large room with no objects in the line of sight but with many objects in the vicinity of both the transmitter and the receiver. To avoid interference from multipath in this measurement setup, and throughout the processing, they only used the main lobe of the temporal and spatial impulse response as shown in [13]. By cutting out the interference, as well as the side lobes, they made it so that the processing done by the CLEAN algorithm is incapable of distinguishing between a new arrival, and the side lobe of a

larger arrival. Also, the magnitude only processing of the PSF hides arrivals whose phase causes them to be masked under portions of other arrivals. Spencer's data also has a significant amount of signal dependent clutter, which they countered by using the CFA detection. Again, weaker arrivals are lost using this approach. None of these problems, however, were as bad as those present in the 2.4 GHz system results. The more widely spaced clusters, the smaller number of rays, and the lower dynamic range, all reduced the effects of these errors in the data presented by Spencer et. al.

3.2 A 6 GHz System

A second system is setup to measure the angle of departure as well as the angle of arrival for multipaths in a wireless channel. This information is crucial for simulating channels with antenna diversity at both the transmitter and the receiver. For these measurements a 6 GHz continuous wave signal is used. While the continuous wave system does not provide time of arrival information, the purpose of this experiment is to map transmit and receive angles for the most dominant arrivals.

3.2.1 Measurement Methodology

An HP8720B network analyzer is used to measure the S_{21} frequency response of the channel at 6 GHz (single frequency measurement) The receive antenna is swept 360° and the signal is measured at 1° increments. For each sweep of the receive antenna the transmit antenna is rotated 10°. In this way the signals received are assigned a transmit and a receive angle.

The signal magnitude and phase measured for each transmit and receive angle represent the sum of all the multipath arrivals that would have been generated with the same transmit and receive angles. If the measurements taken with the first system are collapsed in time (integrate all the signals with respect to time), then the resultant data set would represent all the power received in one sweep of the receive antenna. However, since the first system used an omni-directional transmitter, the angle of transmission would not be available. If the measurements for the second system are also collapsed, but in transmitter angle (integrate all the signals with respect to

transmit angle), then the resultant data set would be the same type as the collapsed measurement from the first system. Both would show all of the power arriving at each receiver angle with, effectively, an omni-directional transmitter.

3.2.2 Hardware Setup

Much of the equipment for this system is borrowed from the 2.4 GHz system described previously. The omni-directional transmit antenna is replaced by a horn antenna with an approximate beamwidth of 36°. The horn is mounted so that it can be rotated over the full 360° at $\frac{1}{36}$ rpm. The receive antenna, the same 90 cm. Eliptical dish used in the other system, is set to rotate at 1 rpm. Having both antennas rotate continuously added some complexity to the data processing as described in Section 3.2.3. The system setup is shown in Figure 3.14. The signal source is again from port

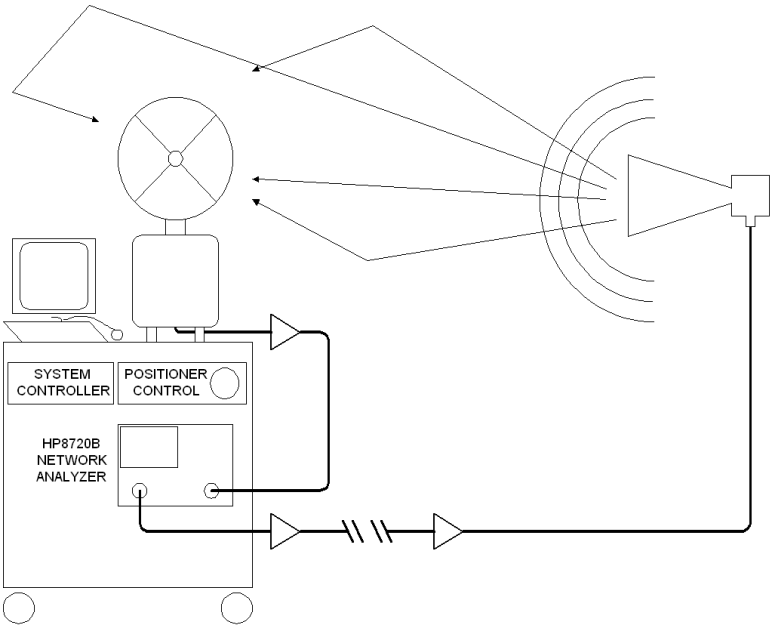

Figure 3.14: 6 GHz System

1 of the HP8720B. The signal is immediately amplified and then sent through up to 500 feet of cable where it is again amplified. The output from the amplifier is fed

into the horn antenna and transmitted to the receive antenna. The received signal is amplified for the final time and then measured by the network analyzer.

The antenna pattern of the receiver is measured on the Clyde Building antenna range as shown in Figure 3.15. The antenna pattern is asymmetrical and has a very

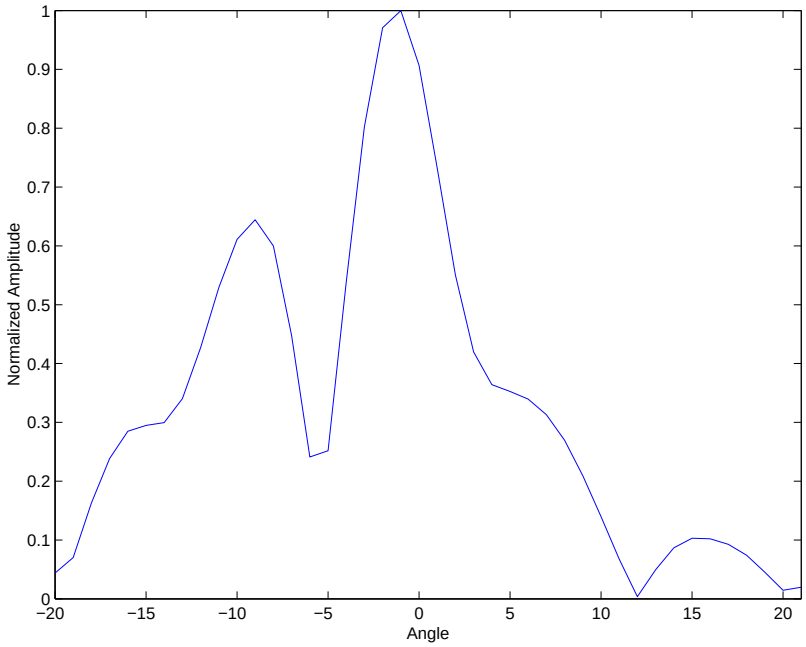

Figure 3.15: Receive Antenna Response

large sidelobe. This large sidelobe makes it appear that there is an object interfering with the measurement. By repeating the measurement and moving the antennas, it is shown that there are no interfering objects and that the antenna does indeed have a distorted pattern at 6 GHz. The hardware for the transmit antenna is difficult to put on the antenna range so the antenna pattern of the transmitter is instead calculated based on its size and geometry as shown in Figure 3.16. This decision is justified because the horn antenna has a simple geometry and is operating in its normal frequency range. By combining the two antenna patterns, the system PSF, shown in Figure 3.17, is generated.

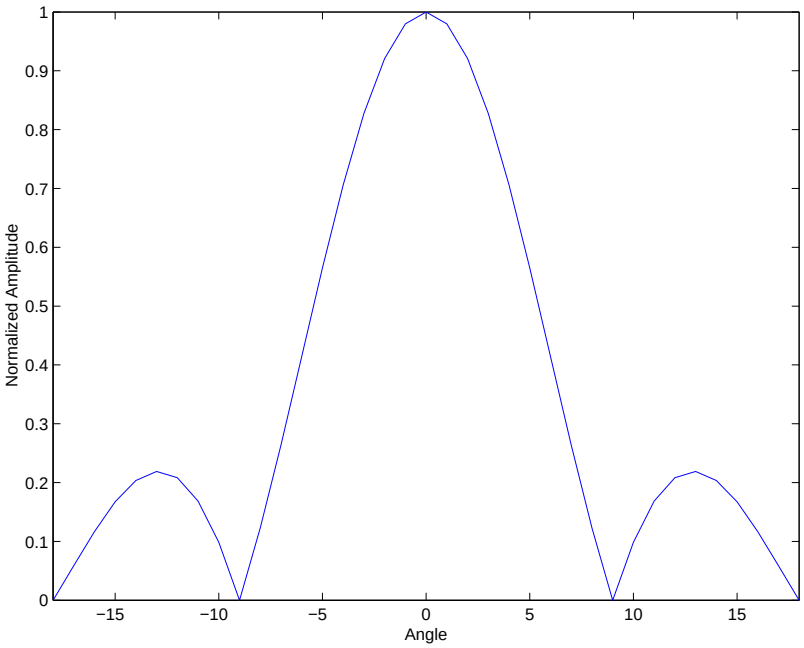

Figure 3.16: Transmit Antenna Response

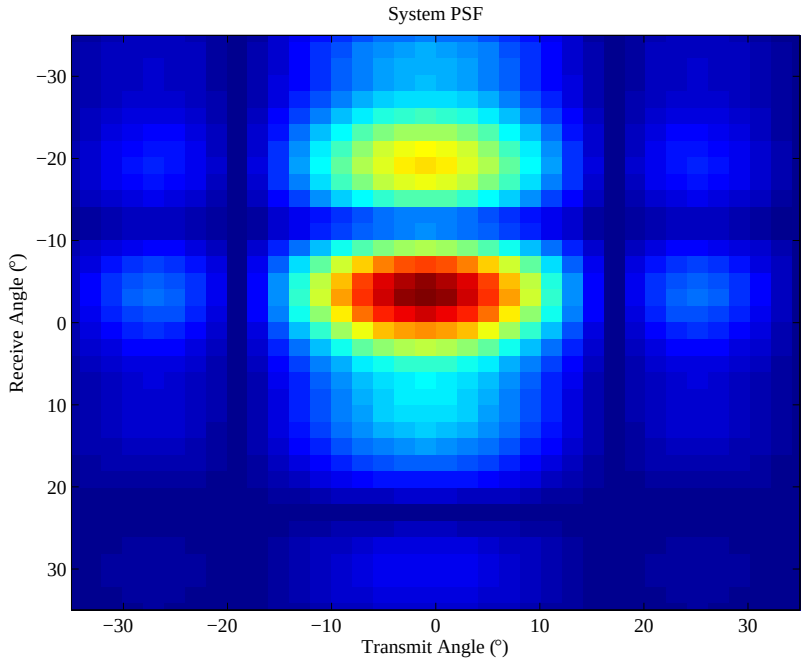

Figure 3.17: System PSF

Another weakness of the system exists in the method that the antenna is rotated. Measuring the antenna pattern for the CW system reveals that the center of rotation for the receive antenna mounted on the positioner is not the antenna phase center. That means that the measured phase of the signals does not represent the phase at the same point in space for the entire measurements. This invalidates one of the initial assumptions, which is that the signals received at each angle, when combined, represent the signal that would be received at a single point. Further investigation shows that the phase center for this antenna varies significantly with frequency and in any case, is too far from the center of mass of the antenna to warrant attempting to rotate around the phase center. The effects of the misalignment between the center of rotation and the phase center can be characterized and removed from the data by re-measuring the phase data in all of the measurements. An even better approach is to use simple parabolic antennas built for the use at 6 GHz. These phase error effects can be accounted for by the deconvolution of the PSF from the data sets in the 2.4 GHz measurement processing if phase information is included in the deconvolution. For the 6 GHz system, rather than remeasure and correct for these errors, the deconvolution is done manually. Only the major returns are identified for these preliminary measurements. The same type of measurements have been continued [14] using better antennas, thus avoiding this problem completely.

3.2.3 Data Processing

The 6 GHz system provides two dimensional images with angle of transmission and angle of reception as the axes. Due to the hardware configuration, both antennas are actually continuously rotating during the measurements. The measurements occur every 1° in the receiver angle, but since the transmitter is also rotating during the measurements, each consecutive measurement (1° step in the receiver angle) has approximately .028° added to the transmit angle. The offsets in the transmit angle for each receiver step add together until the last measurement of a sweep is 10° off from the first measurement. To completely correct for this, the results must be interpolated and re-sampled so that each successive sweep lines up. For this approach to

work, the signal must be adequately sampled in angle. For this system, the limiting components for spatial resolution are the antennas. The beamwidths of the antennas are broad enough that the 10° sample spacing in the transmit angle is more than adequate. Figure 3.18 shows a typical measurement. The brighter red and yellow

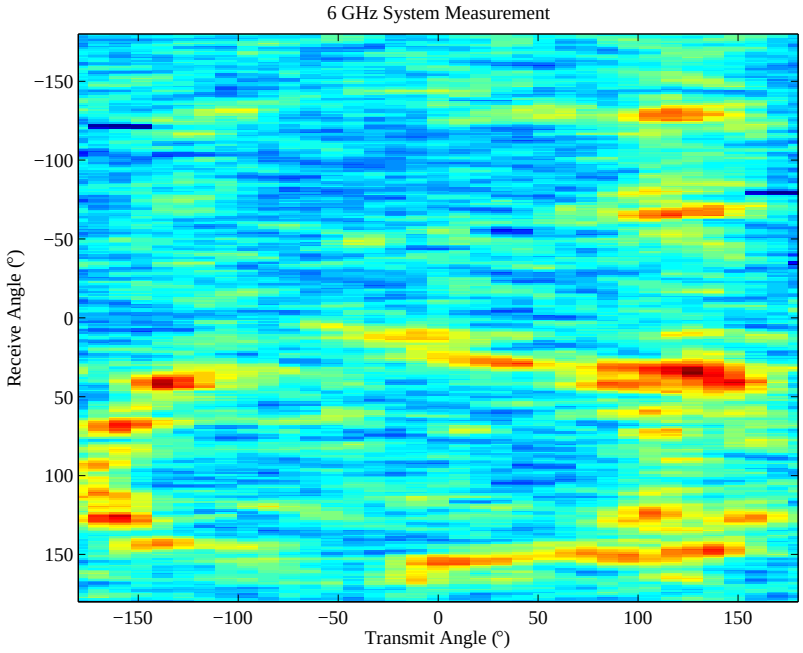

Figure 3.18: Spatial Correlation

features show the spatial correlation evident in this data. This also verifies that even with the moving transmitter, the sample spacing is able to reveal the multipath structure. This is not to say that the antenna beamwidth is not hiding other features, but that given the hardware used, the sample spacing is acceptable. The result of this processing is an image with the received power as a function of the transmit and the receive angles.

After the re-sampling process, the effects of the system blurring had to be taken into account. In much the same way as for the previous system, the CLEAN algorithm can deconvolve the PSF from the image. In this case, however, there is no

need to accurately determine the exact time and amplitude of the arrivals, but just to pinpoint the angles associated with each major signal path. With these simpler goals, as well as the smaller number of measurements, it was deemed unnecessary to actually deconvolve the PSF from the measurements, but instead the points were chosen manually.

As the data sets were taken it was quickly realized that the 6 GHz system could not provide usable results over the same physical separation range as the 2.4 GHz system. Even after switching to shorter cables with less loss, the signal to noise ratio was often very low. The reason for this problem is that the cables and amplifiers used for both systems are much less efficient at 6 GHz. To partially overcome the low signal to noise ratio, a smoothing, or spatial averaging function is applied to the image. Figure 3.19 shows one data set before and after smoothing. The filtering applied to suppress the noise is a simple two dimensional convolution of a rectangular window of ones (W) with the image, as given by [15],

$$I_{smoothed}(n_1, n_2) = \sum_{k_1=-\infty}^{\infty} \sum_{k_2=-\infty}^{\infty} I_{raw}(k_1, k_2) W(n_1 - k_1, n_2 - k_2), \tag{3.3}$$

where I is the image data and W is the two dimensional rectagular window used to smooth I_{raw}. This reduces the noise [16], and leaves the most significant features exposed. Of course this smoothing slightly distorts the signals, but the ability to pick out the major paths and ascertain the transmission and reception angles is increased. This approach works because each arrival is the convolution of an ideal point arrival with the system PSF. Performing the spatial averaging with a window smaller than the PSF will average out the higher "frequency" noise without significantly distorting the PSF shape. Weaker arrivals, however, that are too close to the noise floor will be lost using this approach. More complex algorithms using the PSF can be devised for more thorough processing.

3.2.4 Measurement Results

Thirty data sets were taken with this measurement setup. The correlation between consecutive revolutions of the receive antenna (one transmit angle to the

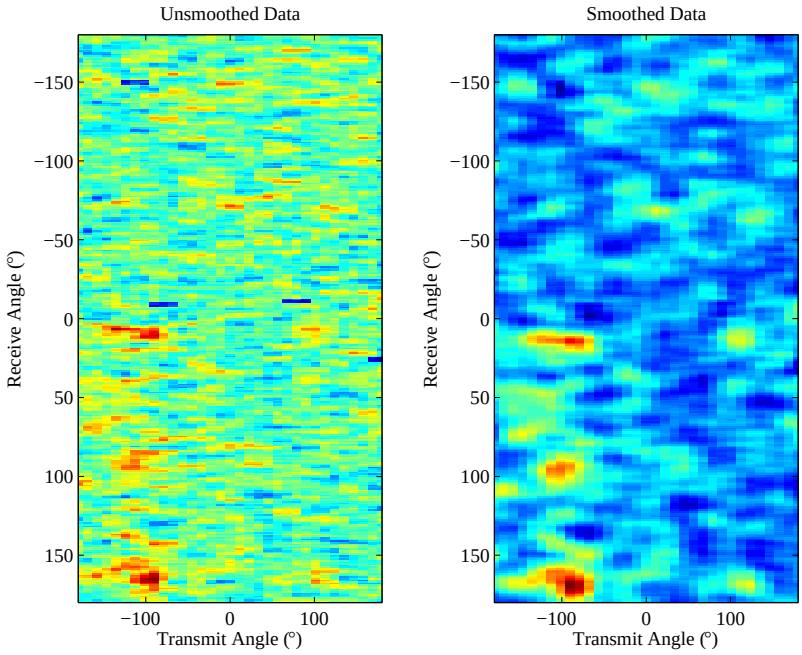

Figure 3.19: Noise Suppression

next) is very good. This indicates that the spacing of the transmit antenna angles adequately samples the channel, given the resolution of the hardware used. There is no problem in identifying the major returns in the data. Figure 3.20 is an image showing a set of data that was taken with the source and transmit antennas in adjacent rooms with approximately 50 feet of separation. Each of the major returns are easily traceable to features in the room. Just as in the case of the 2.4 GHz system, the accuracy and stability of the PSF limits the ability to resolve many more features. Two other measurements are shown in Figures 3.21 and 3.22. In each case the major returns are easily isolated and give a very good picture of the transmit and receive angles for the multipath.

These measurements show that the 6 GHz system is able to measure the angle of transmission and reception for multipath in an indoor environment. This is the first step in being able to characterize angle of departure statistics and add them to the modified Saleh and Valenzuela model. These measurements can also be

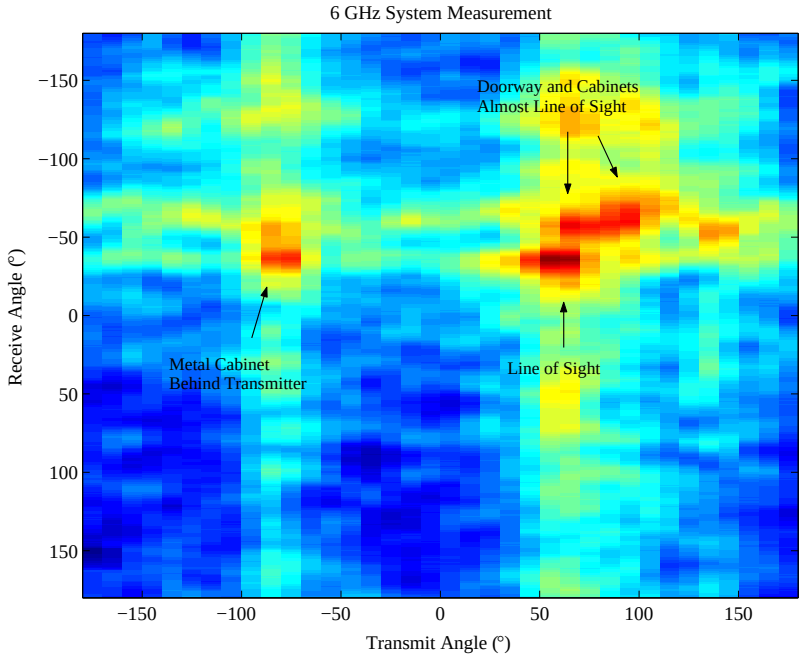

Figure 3.20: Arrival Mapping

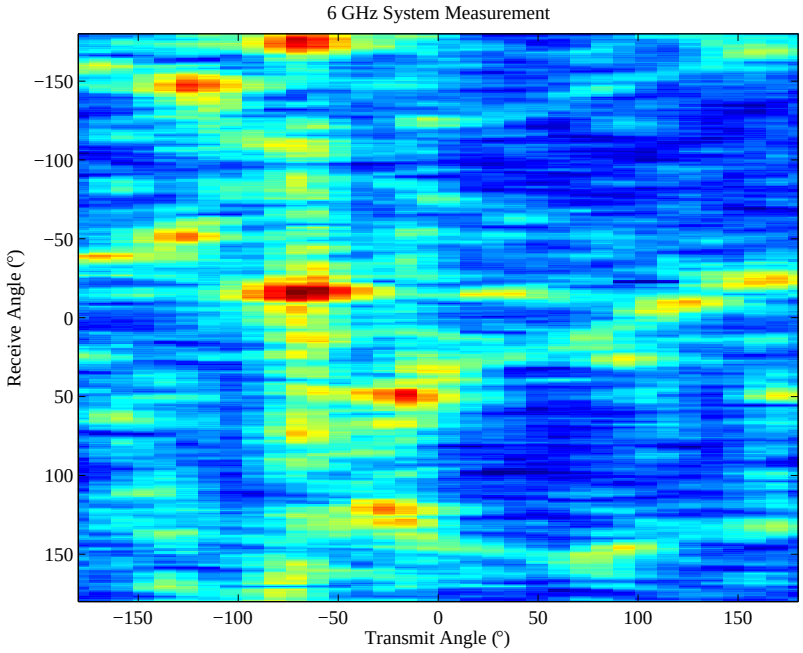

Figure 3.21: 6 GHz System Measurement A

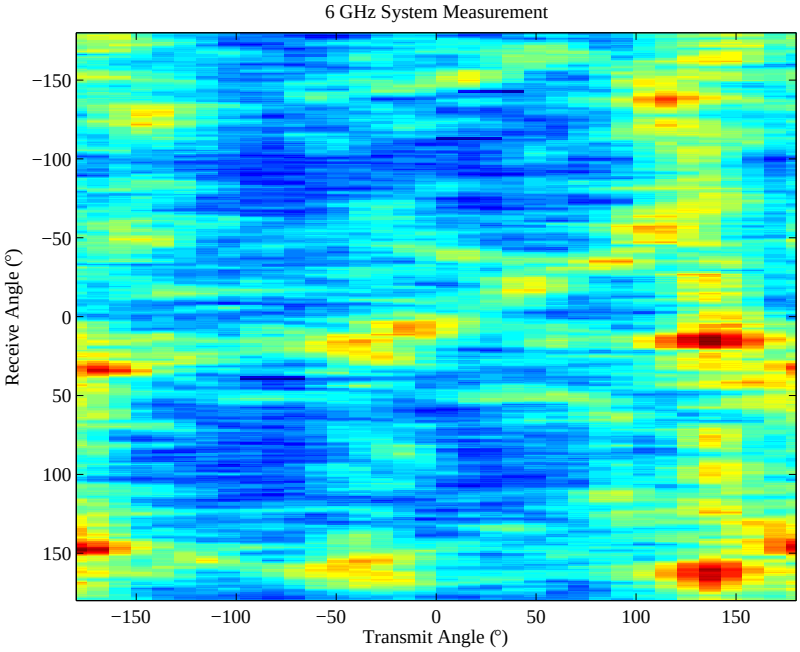

Figure 3.22: 6 GHz System Measurement B

used to construct the transfer matrix of an arbitrary arrangement of transmit and receive antenna configurations for a MIMO channel. Ted Pyper helped make the 6 GHz system measurements and then used this same concept as well as much of the same equipment to make improved measurements of the 6 GHz channel. His measurements, although taken later, were published before this work in [14]. From these measurements he created channel matrices for various antenna configurations and compared them to a direct MIMO probing approach.

Chapter 4

Clustering

The models presented in Chapter 2 are based upon the experimentally observed phenomenon that multipath arrivals appear in clusters. In order to capture the statistical behavior of these clusters as well as the arrivals within them, some sort of clustering or grouping algorithm must be applied to the measured data. Errors in cluster identification or inconsistency in data processing can lead to variations in the extracted model parameters [17], [18]. In this chapter, different automated clustering algorithms are investigated and their accuracy in parameter estimation is determined. Additionally, the sensitivity of channel characteristics to parameter variability is assessed. In particular the channnel characteristics most relevant to MIMO communications, derived from the channel model, are examined.

4.1 Clustering Methods

In [1] Saleh and Valenzuela measured the temporal structure of the multipath arrivals. In processing the data they manually identified the various arrival clusters and subsequently estimated the statistical parameters describing these clustered arrivals as detailed in Chapter 2. This simple approach forms the foundation of the more sophisticated algorithms explored here.

It is important to emphasize that cluster identification and statistical characterization must be performed on the data after it has undergone deconvolution and post-processing as outlined in Chapter 3. In order to avoid inaccuracies involved with this processing, all data used for analyzing the clustering methods is generated using the extended Saleh and Valenzuela model presented by Spencer et. al. [2]. This

makes it possible to quantify the errors of each clustering method by comparing the results to the generated "true" data.

One problem with using this model to test the clustering process is the generation of overlapping clusters. While this is also seen in the actual measured data, the model is able to output overlapping arrivals with arbitrary amplitudes that would be indistinguishable to the CLEAN algorithm used for deconvolution. The model's ability to generate these arrivals is not necessarily an error or misrepresentation of the signals that would truly be present in a channel, but represents a portion of data that is lost in physical measurements. This can be verified by analyzing more isolated clusters where the presence of the smaller arrivals is not overshadowed by larger arrivals in another cluster. Figure 4.1 shows an example of one isolated cluster, and two overlapping clusters. From the isolated cluster, an estimate of the typical spread

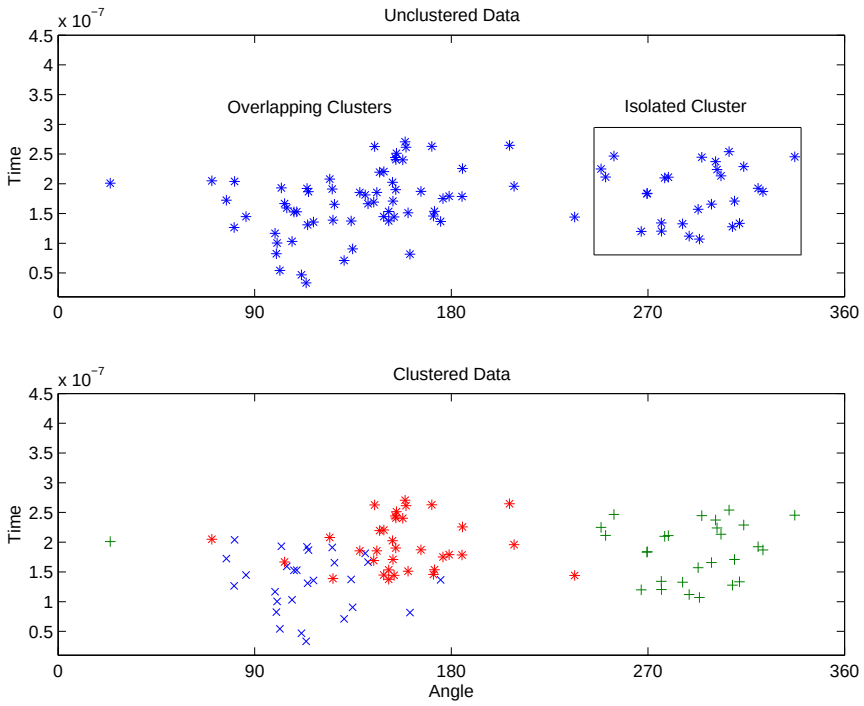

Figure 4.1: Isolated and Overlapping Clusters

in angle and time can be seen. The ability to separate the overlapping arrivals into the appropriate clusters is one of the motivating factors for the clustering techniques presented in this work. The performance of these clustering algorithms is assessed in Section 4.2.

4.1.1 Arrival-by-Arrival Method

The simplest method of clustering is to individually select each arrival and assign a cluster number to it. By clustering in this manner, the angle, time, and amplitude of each individual arrival can be taken into account when determining which cluster it should be assigned to. A major disadvantage of this method is its tedious nature. Except in the sparsest of multipath environments or in the case of very few measurements, this method is not feasible. Another problem is the potential inconsistency when assigning the arrivals to clusters, particularly for arrivals that may lie between clusters. The alternate clustering methods presented here are designed to minimize the manual processing required and thereby improve the repeatability of the results.

4.1.2 Rectangular Method

In [2] a Matlab interface was used to graphically plot the arrivals on a two dimensional image, with the angle and time of arrival used as the horizontal and vertical axes, respectively. The arrival amplitude was indicated according to a color map. With all arrivals displayed, rectangles were manually drawn around each cluster. This same method is adapted slightly and used in the initial analysis of the 2.4 GHz measurements as discussed in Chapter 3.

The visual determination of cluster boundaries both in angle and time is very similar to the process followed by Saleh and Valenzuela for determining boundaries in time. This method is a very simple and efficient way to be able to correctly separate the majority of arrivals into clusters. Figure 4.2 shows a typical set of arrivals marked over the raw data image where the color is indicative of the amplitude, and Figure 4.3 shows the arrivals without the image in the background. Figure 4.4 shows the

rectangular boxes drawn around each cluster of arrivals. The clustering for this method can be done with (Figure 4.2) or without (Figure 4.3) the image in the background.

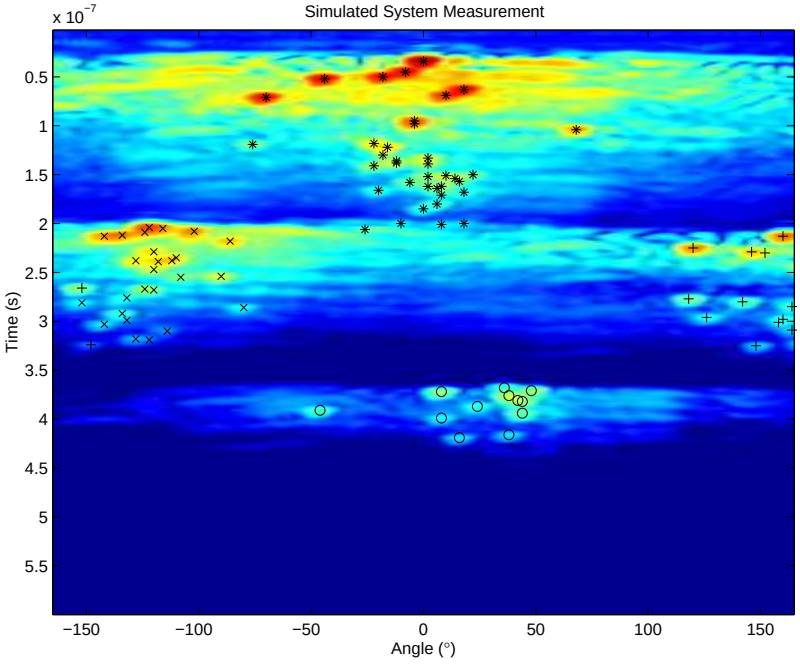

Figure 4.2: Arrivals on Simulated Measurement

Despite the many arrivals in this example, the multipath clusters happen to be well spaced so that most arrivals are correctly clustered. When the clusters overlap in angle and time, due to more arrivals or more closely spaced clusters, the percentage of errors goes up significantly (Section 4.2). One problem with this method is that the clusters are limited to what can be uniquely identified in rectangular regions. If clusters appear immediately adjacent to each other on the image, a line of separation must be chosen and any arrivals from each cluster that extend beyond the line will be incorrectly assigned.

A second significant problem with this method is the repeatability of the clustering process. If the same data set is presented multiple times the cluster results

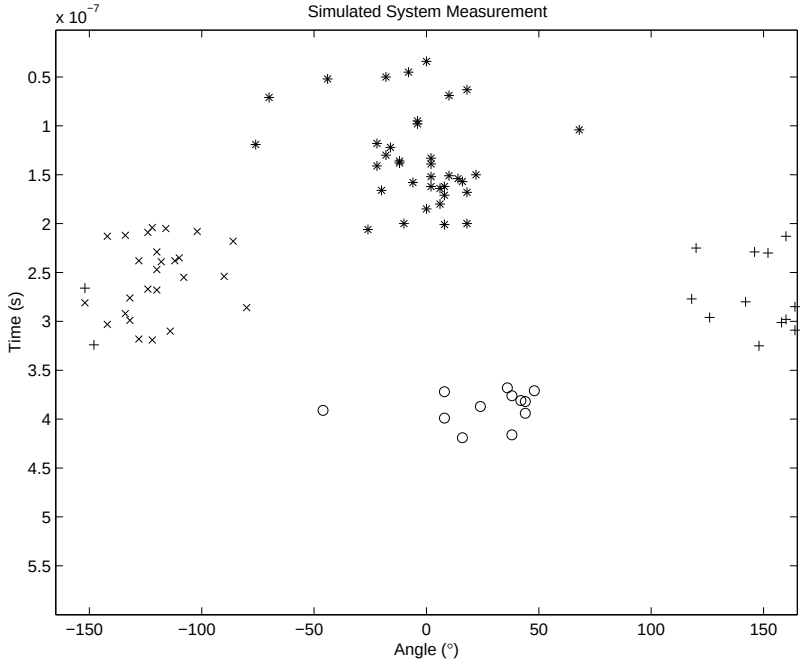

Figure 4.3: Simulated Arrival Locations

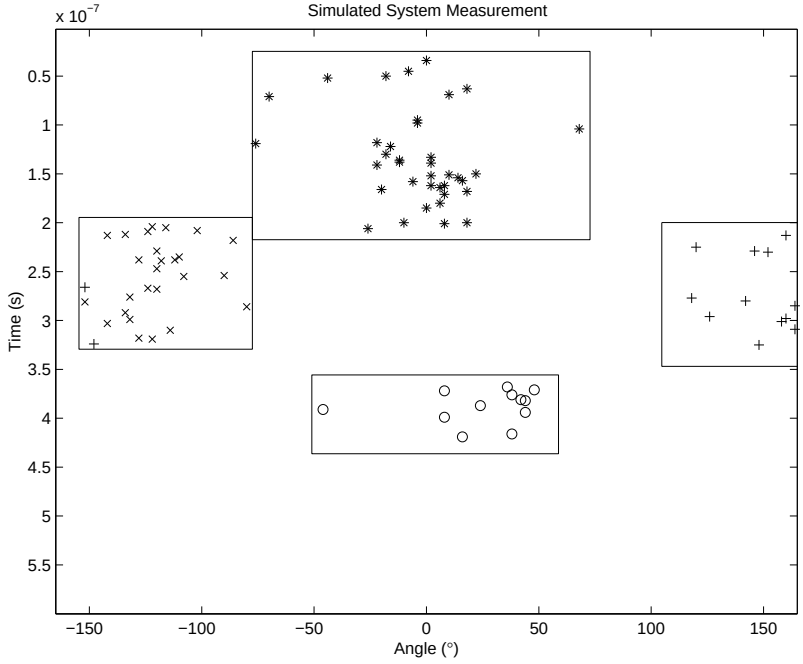

Figure 4.4: Clustered Arrivals

can be different for each trial. Variation from user to user can be even more significant. For example, in learning to use the method, the operator must first guess the typical dimensions of a cluster. Whatever assumptions are made at this point will tend to influence the dimensions of future clusters. When applying this method for comparison, great care is taken to try to be as unbiased as possible in clustering the arrivals. Any variation in the selection of boundary locations can cause a change in the statistics derived from the data.

During use of this method for analyzing the 2.4 GHz system results, it was observed that the clustering could significantly impact the parameters extracted from the data for use in the model. The rectangle dimensions impact the angular and temporal spread parameters for the cluster. The arrivals that are incorrectly combined into the end of a cluster will tend to alter the amplitude distribution. Arrivals left out of the correct cluster may cause the formation of a false cluster, which will also impact the statistical parameters.

It must be stated that once an operator has experience in performing this task, it is possible to select the clusters more consistently. Also, some of the errors due to overlapping clusters tend to cancel rather than add. For example, two overlapping clusters being divided may result in one that is too wide and one that is too narrow. The arrivals that are incorrectly clustered are often the lowest amplitude in the cluster and therefore have a smaller effect on the final results. Finally, the images that have several clusters closely spaced often have enough arrivals to statistically cover up the errors in clustering. The percentage of errors does increase, but not necessarily by a large amount.

4.1.3 Fuzzy Distance Method

The Fuzzy Distance Method uses fuzzy c-means clustering [15], [19], [20], [21] to assign the rays to clusters. It was developed to allow the cluster boundaries to vary in shape and size according to the trends in the data. In this approach, the approximate location of each cluster center is entered into a Fuzzy Clustering algorithm based on the fuzzy c-means clustering provided in Matlab. The algorithm

tries to minimize the distance from the cluster center to the points within the cluster. Each point is assigned to the cluster center which minimizes the Euclidean distance

$$d = |\overline{r} - \overline{r}_{c_i}|, \tag{4.1}$$

where $\overline{r}$ and $\overline{r}_{c_i}$ are the locations of the arrival and the center of the i^{th} cluster, respectively, in the angle-time space. The centers $\overline{r}_{c_i}$ are then moved around until a predetermined distance threshold or number of iterations is reached. It is important to emphasize that $\overline{r}$ and $\overline{r}_{c_i}$ represent a vectors mapped onto angle and time axes. While using the euclidean distance in the angle-time space does not make sense physically, the distance to a cluster center is a very accurate way to assign clusters.

The cluster centers are moved around using the "fcm.m" file in matlab. During each iteration, the distance of each cluster center to neighboring arrivals is reduced, with a bias towards moving closer to nearby arrivals rather than arrivals that are farther away. The cluster centers follow the gradient towards local minima. This is important since minimizing the overall distance to all arrivals could result in all of the cluster centers being co-located at the center of the largest cluster. One drawback to this approach is that two centers that randomly start far away from most arrivals may move towards and "share" the arrivals of the closest cluster available. It is for this reason that the algorithm was modified so that the user inputs initial locations for the cluster centers.

One of the key benefits of this method is the elimination of the tedious selection of arrivals for each cluster. The designation of the cluster centers does not need to be performed with high precision and involves simply clicking a few times on each image. This is in contrast to the procedure of drawing rectangles, which requires additional decisions to be made. This is especially useful for cases where 2 or more clusters overlap and must be divided into individual clusters.

This process is also much less user dependent and significantly improves the repeatability of the clustering. Several attempts were made to eliminate the manual process of center identification, but the clustering algorithm is more repeatable if the cluster centers start in approximately the correct location as opposed to a random

center placement. Also, this step provides the algorithm with the total number of clusters to be created. Attempts to have the algorithm choose the number of clusters are successful in about 90% of the cases, but result in large errors in the failed cases. Due to the relative ease of performing this one step by hand, it is left as part of the process. If a large number of measurements need to be clustered using this algorithm, it would be valuable to spend more time automating the cluster center identification.

Along with the improved repeatability of the measurements, the Fuzzy Distance Method allows more flexibility in setting cluster boundaries. This method effectively draws lines of demarcation perpendicular to the lines between cluster centers. Therefore the cluster identification boundaries are general polygons, not simple rectangles. Additionally, cluster sizing is automatically accomplished. However, the separation lines still do not allow overlapping clusters. In order to accomplish this, amplitude information for the arrivals must be incorporated. This fact can lead to clustering errors. For example, a very small arrival at the tail end of one cluster is consistent with the model. However, if the arrival is closer to an adjacent cluster center, it will be incorrectly clustered.

Another problem with this method (that did not exist for the manual "rectangular" cluster identification process) is that it can lead to improper splitting of non-overlapping clusters. Due to the nature of the Fuzzy Clustering used, both axes are treated as units of distance. Each arrival is assigned to a cluster based on how far it is, both in angle and time, from the cluster center. If the clusters are more spread out in time than in angle, some of the arrivals will be assigned incorrectly. For example, sometimes clusters can be next to each other in angle, but offset in time of arrival. Even with no overlap of the two clusters, the distance method can group the tail of one cluster into the nearby (incorrect) cluster. This occurs when the typical angular spread of a cluster generated from the model is smaller than the typical temporal spread, or vice versa. The fuzzy clustering code evenly weights a separation in angle with a separation in time, so that even if the clusters do not overlap visually, the algorithm can divide them incorrectly based on overall distance. This is partially corrected by scaling the time variable appropriately so that the variance of a cluster

of arrivals in time is approximately the same as the variance of a cluster of arrivals in angle. This equalization of the variances causes a typical cluster of arrivals to be relatively circular when plotted in the angle-time space.

4.1.4 Fuzzy Weighted Distance Method

The Fuzzy Weighted Distance Method is a variant of the approach discussed above. As described previously, the Fuzzy Distance Method does not use the amplitude information to cluster the arrivals. The rectangular method allows the operator to consider the amplitude in determining the placement and size of the rectangles, but in either method the cluster boundaries are delimited on the image plotted on the angle and time axes. While these are very reasonable approaches, it is easy to extend this one step further. This method, like the previous one, uses the distance from the cluster center as the determining factor for cluster assignment. The approach is modified here to appropriately include the arrival amplitude to reduce the distance of each arrival from the correct cluster center by offsetting the temporal spread of the cluster. For example, it is reasonable to assume that a very small arrival near the end of the first cluster and the beginning of a second cluster is more likely part of the previous cluster, even though it may be closer to the second cluster center. This can be assumed because it is known that the amplitudes of the arrivals within a cluster tend to decay with time. The lower amplitude arrival could be shifted back in time so that it is easy to see that it is indeed part of the previous cluster. This does not guarantee that the small arrival described is not just a statistical anomaly, and truly part of the second cluster, but that scenario is less likely.

To properly use arrival amplitude information to determine cluster assignment, we must first recall from our models that arrivals within a cluster tend to have amplitudes that decay exponentially in time. Therefore, an arrival that has a small amplitude will tend to have more delay than one with a larger amplitude within the same cluster. The approach proposed here uses the relationship between the amplitude and delay of an arrival to map arrivals into a new coordinate frame in which the

cluster structure is more clearly defined. The average arrival amplitude is given by

$$\overline{\beta}_{kl} = \overline{\beta}_{00} e^{-\frac{T_l}{\Gamma}} e^{-\frac{\tau_{kl}}{\gamma}}, \tag{4.2}$$

as described in Chapter 2. Taking the natural logarithm of both sides and rearranging the terms results in

$$-\frac{\gamma T_l}{\Gamma} = \gamma \ln(\frac{\overline{\beta}_{kl}}{\overline{\beta}_{00}}) + \tau_{kl}, \tag{4.3}$$

where $\overline{\beta}_{00}$, Γ, and γ are constants for a given channel and T_l is a different constant for each cluster. The left side of Equation (4.3) is now a cluster dependent constant, while the right side contains the amplitude and arrival time of the signal. This relationship leads to the change of the vertical axis

$$y = t, \tag{4.4}$$

to

$$y = \ln(\frac{\beta_{kl}}{\beta_{00}}) + t, \tag{4.5}$$

where $\frac{\beta_{kl}}{\beta_{00}}$ is the normalized arrival amplitude and t is the delay.

Using this new time:amplitude mapping, each arrival within a cluster, is mapped to roughly the same constant value on the vertical axis. Figure 4.5 graphically shows the exponential relationship between the time and amplitude of the arrivals without the new mapping. The clusters are color-coded in this figure, however, when such data is obtained experimentally, the severely overlapping clusters result in significant cluster assignment errors if time alone is used to delineate the clusters. By plotting the same data using Equation (4.5) to obtain a time:amplitude vertical axis, the clustering becomes much more straight forward. Figure 4.6 shows the final translated values plotted against time. Each cluster has a unique value on the vertical axis. The values for each arrival within a cluster are not exactly identical due to the randomness of the amplitudes about the double exponential curves, as described in Chapter 2. However, the similarity of the amplitudes facilitates the clustering process.

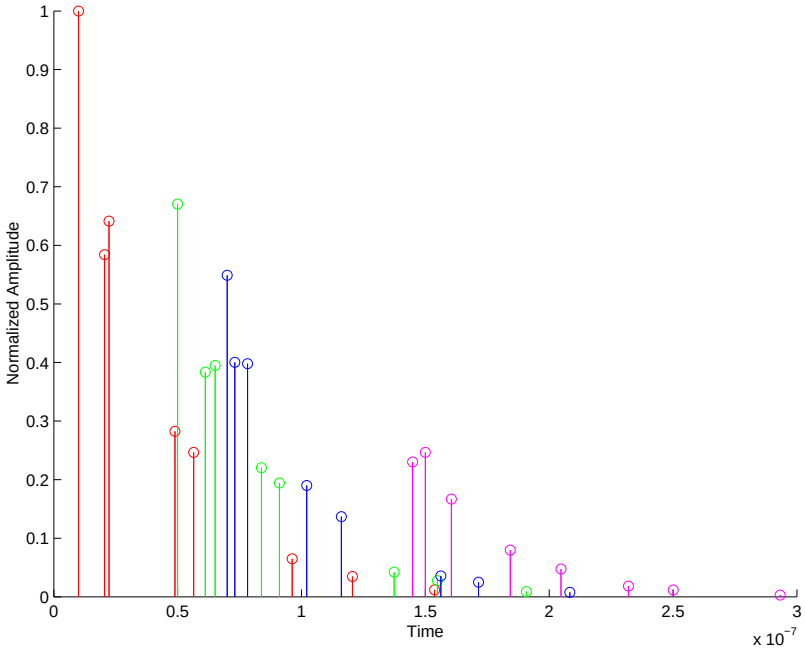

Figure 4.5: Arrival Data

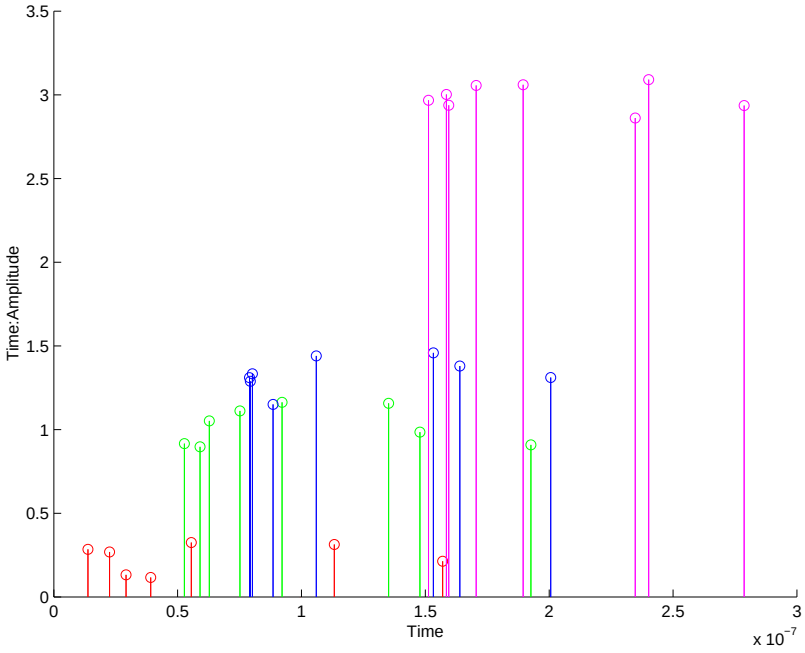

Figure 4.6: Logarithm of Amplitude + Time

At this point the Fuzzy Distance Method described in Section 4.1.3 is used. The arrivals are plotted on the angle and time:amplitude axes, and the approximate cluster centers are chosen. The algorithm moves the centers around until the Euclidean distance (Equation (4.1)) of the arrivals from their respective cluster centers is minimized to within a certain threshold or a maximum number of iterations is reached. Also, as with the Fuzzy Distance Method, a scaling factor is introduced to equalize the variances of the arrival clusters on both axes.

This method, while not perfect, is able to correctly cluster many arrivals in synthesized data that are incorrectly clustered by the other methods (Section 4.2). Using this approach, clusters that overlap each other by more than 75% can often be completely resolved. In most cases there are only a few errors that occur when the randomness of the amplitude causes some arrivals from one cluster to lie closer to the amplitude curve of another cluster, and the angles are close enough together that they cannot be distinguished. The only situation that results in significant errors compared to the known true clusters in the generated data is when the two clusters arrive at nearly the same time and the same angles. In this case, with measured data, the clusters would be seen as the same cluster. Without the a priori knowledge of the true clusters, the fact that the arrivals are more densely packed in the area is the only indication that they are not in fact the same cluster. This method is even more accurate than hand selecting each arrival and placing it into clusters, since it takes into account the minute variations in the time:amplitude variable that are not easily distinguishable when looking at the angle, time and amplitude separately.

4.1.5 Weighted Rectangular Method

The Weighted Rectangular Method uses manual cluster selection on images showing the angle versus the time:amplitude function. Since this new image maps the time:amplitude on the vertical axis, the clusters appear very tightly clustered and manual rectangular delineation works nearly as well as the fuzzy clustering delineation in many cases. There is little reason for choosing this method since it is more work than the Fuzzy Weighted Distance Method and not quite as accurate. It is used

only to help determine how much benefit is gained by being able to use the Fuzzy Clustering algorithm rather than selecting the clusters manually.

4.2 Effects of Cluster Errors

The goal of each method of clustering is to minimize the errors in cluster assignments. Since each arrival in a cluster contributes to the parameter estimation for the model, any assignment errors can change the parameter results. A comparison of three of the clustering methods is provided here to demonstrate their relative performance. In this comparison, the Rectangular Method (RM), the Fuzzy Weighted Distance Method (FWDM), and the Weighted Rectangular Method (WRM) are used to cluster the same model-generated data sets and the results are compared to the true clusters. After quantifying the errors in parameter estimation, the effects of these errors on the simulated data are demonstrated. In particular the statistics of model-generated channel matrices are analyzed for a wide range of model parameter values [22]. In this manner, the typical model parameter errors are translated into the statistical changes in random channel matrix generation. Furthermore, the channel capacity computed from these channel matrices, using the water filling solution, is evaluated to show the sensitivity of the capacity to the model parameters.

4.2.1 Parameter Estimation Errors

To compare the algorithms, a trial measurement campaign is run with 100 sets of generated data. Each set is clustered using the RM, the FWDM, and the WRM. Figures 4.7 - 4.9 show one data set being clustered by each method. The clusters are mapped repeatedly between -540° and 540° to allow for better visualization of the cluster shapes as the angle wraps around 360°. In this particular data set, the RM assigns four clusters (Figure 4.7). With the data displayed on the time:amplitude versus angle axes (Figures 4.8 and 4.9), it is apparent that there are more than four clusters, demonstrating one benefit of using this mapping. Figures 4.10 and 4.11 show the final clusters on the time:amplitude and time axes respectively. The "true" clusters are also included in these figures for reference. As shown by the final cluster

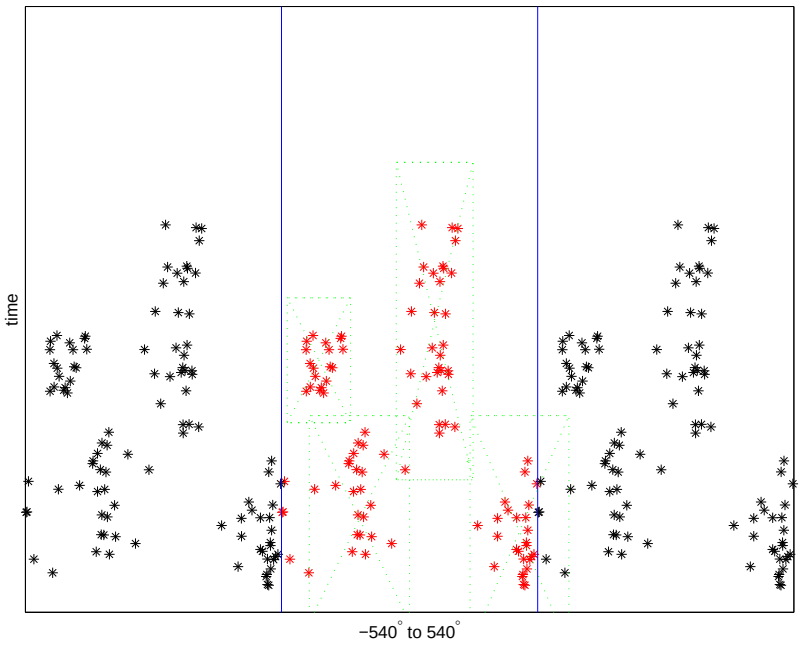

Figure 4.7: Rectangular Method

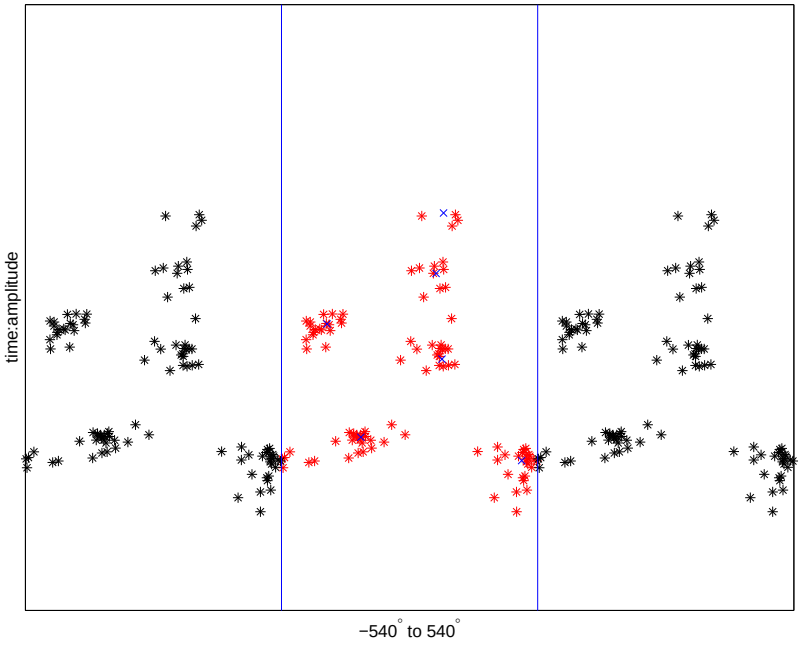

Figure 4.8: Fuzzy Weighted Distance Method

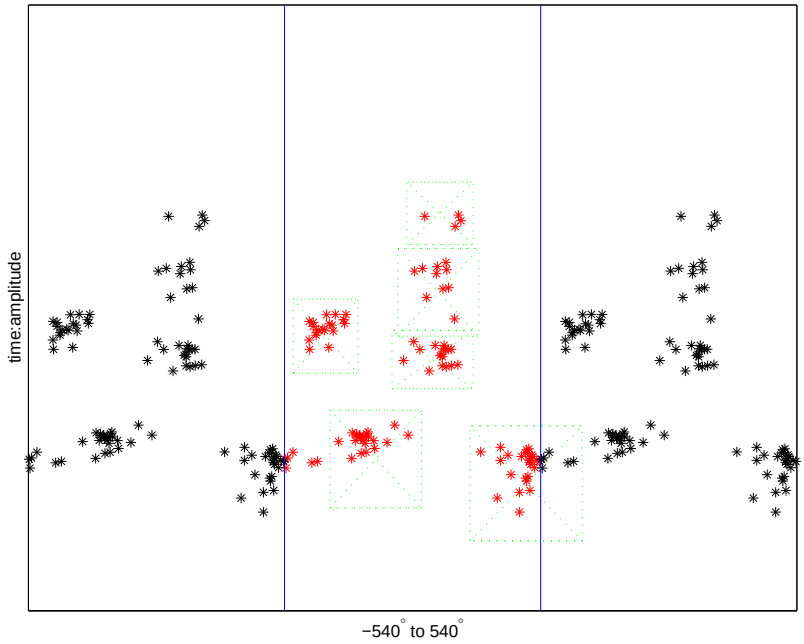

Figure 4.9: Weighted Rectangular Method

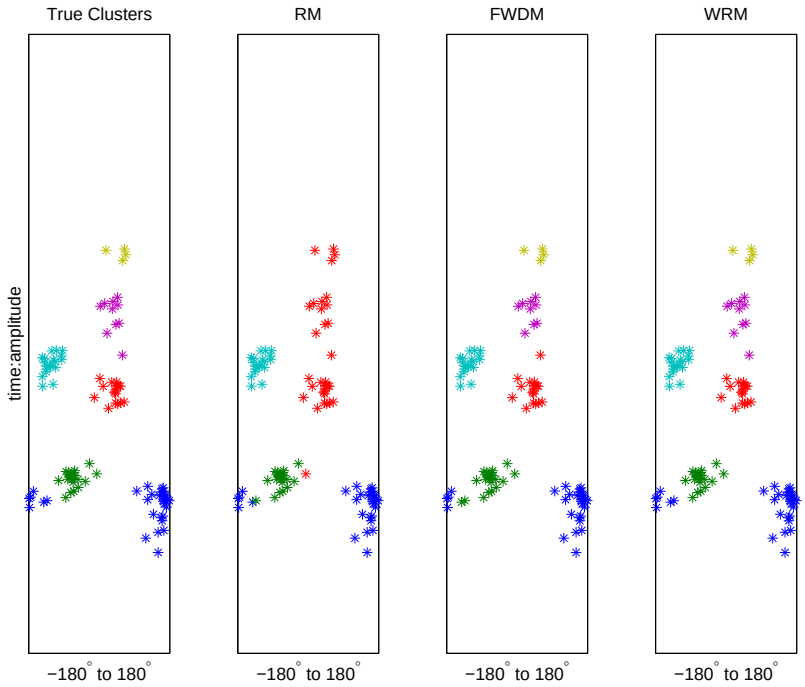

Figure 4.10: Final Cluster Assignments (vertical axis = time:amplitude)

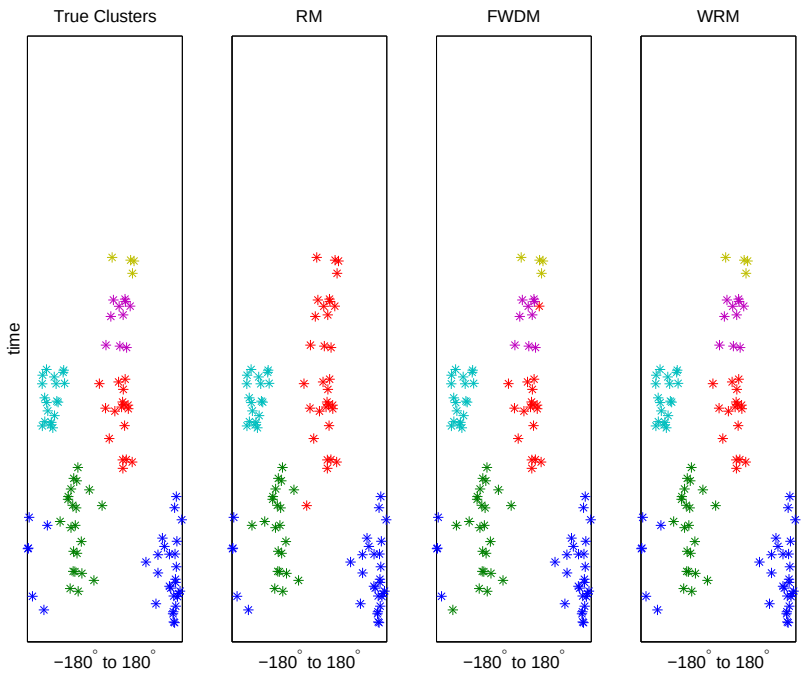

Figure 4.11: Final Cluster Assignments (vertical axis = time)

assignments, the RM results in multiple cluster assignment errors, the FWDM has 3 errors, and the WRM clusters the arrivals perfectly.

As with any Monte Carlo simulation, a finite sample size may not generate the "exact" statistical distribution specified by the input parameters. When this happens, the errors calculated can be altered due to the particular realizations that were used. In an attempt to measure only the errors due to the clustering algorithms, each parameter estimate is compared to the parameter estimate taken from the known "true" cluster assignments. This approach has the added benefit of insuring that any accidental errors in the parameter estimation code are canceled out, as these errors will be common to each set of parameter estimates. An example of this is if the parameter entered for the angular spread is 25°, but the model-generated data shows a 26° spread, the clustering methods should be compared to the 26° spread for a fair analysis. The sample size for these experiments is 100 data sets.

The parameter estimates are each calculated by curve-fitting to the Culmulative Distribution Function (CDF) for each paramter. For the arrival rates, Λ and λ, the Δ times between clusters and arrivals are calculated and the CDF's of these Δ times are estimated by plotting a histogram. The actual rate is then found by fitting an exponential to the histogram curve which is an approximation of the CDF. The decay rates Γ and γ are also found by fitting exponential curves to the combination of all of the time and amplitude pairs for each the clusters and arrivals respectively. The arrival angle variation, Σ, is calculated by curve fitting to the histogram of the relative angle within the cluster. The mean squared value of the Rayleigh distributed amplitudes are given by the double expontials as shown in Equation (2.4).

Table 4.1 shows the error percentage for each of the 5 model parameters described in Chapter 2. The parameter values used to generate the data sets are shown

Table 4.1: Baseline Parameter Values

	Value	**RM Error**	**FWDM Error**	**WRM Error**
Γ	6.0E-08 s	0.3%	-0.4%	0.1%
γ	2.0E-08 s	-27.2%	-3.6%	-2.9%
σ	25°	3.9%	-2.7%	2.7%
Λ	1/300E-9 s^{-1}	19.4%	3.4%	4.3%
λ	1/5E-9 s^{-1}	-0.2%	0.3%	-1.3%

on the left. In this case they are the same as those measured by Spencer et. al. [2]. His parameter values are used as the starting point for all of the following comparisons. From these results it can be seen that the FWDM and WRM are both able to estimate all 5 model parameters reasonably well. The RM also performs well, but is notably worse at estimating the decay rate for rays (γ) and the arrival rate for clusters (Λ). In performing the clustering with the RM, it is often difficult to determine the number of clusters. Usually the number is underestimated resulting in fewer clusters with more arrivals. This causes the cluster arrival rate, (Λ), to be biased higher. The extra arrivals in these clusters do not have the correct amplitudes statistics, so the amplitude decay rate (γ) is also biased.

Several other trials are performed to see how well the algorithms function when the input parameters are changed significantly. In these trials, data sets the are generated and clustered one at a time, and a cumulative parameter estimate for each clustering method is calculated. Each method is used on additional data sets until the estimates converge to stable values. Typically, fifty data sets provide repeatable and stable parameter estimates. The parameters associated with individual arrivals converge much more quickly than the parameters associated with the clusters since there are many arrivals for each cluster. Tables 4.2 - 4.5 show the results of four of these trials.

Table 4.2: Increased Arrival Rates

	Value	**RM Error**	**FWDM Error**	**WRM Error**
Γ	6.0E-08 s	-0.9%	-0.6%	-0.9%
γ	2.0E-08 s	-32.7%	-1.6%	-5.3%
σ	15°	1.4%	-15.2%	2.7%
Λ	1/100E-9 s^{-1}	18.1%	4.0%	12.2%
λ	1/2E-9 s^{-1}	-3.0%	-1.5%	-3.2%

Table 4.3: Decreased Arrival Rates

	Value	**RM Error**	**FWDM Error**	**WRM Error**
Γ	6.0E-08 s	0.1%	-0.2%	0.7%
γ	2.0E-08 s	-10.6%	-1.3%	-0.2%
σ	15°	-5.7%	-5.4%	0.1%
Λ	1/600E-9 s^{-1}	29.8%	18.9%	9.8%
λ	1/10E-9 s^{-1}	-2.1%	-0.8%	-0.3%

In viewing these results, it is important to remember that the scale factors for equalizing the cluster spread on both axes (used in the FWDM and WRM) are based on expected parameter values. For the best results it is necessary to adjust these values for each measurement campaign. For these trials the values are not adjusted.

Table 4.4: Decreased Number of Arrivals per Cluster

	Value	**RM Error**	**FWDM Error**	**WRM Error**
Γ	6.0E-08 s	0.4%	0.4%	0.7%
γ	2.0E-08 s	-16.9%	-2.1%	-3.9%
σ	15°	-1.4%	-2.1%	-6.1%
Λ	1/300E-9 s^{-1}	11.7%	9.3%	10.1%
λ	1/20E-9 s^{-1}	-5.7%	-3.3%	-0.6%

Table 4.5: Increased Arrival Rates and Decreased Decay Rates

	Value	**RM Error**	**FWDM Error**	**WRM Error**
Γ	7.0E-08 s	-1.6%	0.4%	-0.8%
γ	2.5E-08 s	-34.7%	0.5%	-6.3%
σ	25°	5.7%	-2.3%	4.7%
Λ	1/200E-9 s^{-1}	22.9%	5.3%	8.4%
λ	1/3.5E-9 s^{-1}	-3.5%	-1.2%	-2.4%

Table 4.2 shows the performance when the arrival rates for both individual rays as well as clusters are increased and the angular spread is decreased. In Table 4.3 the same arrival rates are decreased significantly from the baseline values without changing the angular spread. The lower number of clusters makes it more difficult for all three algorithms to estimate the cluster arrival rate Λ. For Table 4.4 the cluster arrival rate is returned the baseline from [2], but the number of arrivals per cluster is left at a lower value. Finally, in Table 4.5 the arrival rates are increased and the decay rate is decreased. Both of these changes result in more total arrivals, since the rays come faster and more of the amplitudes stay above the noise floor. The angular spread is also returned to the baseline value.

When comparing the performance of the three methods, some interesting results are observed. The worst error for all estimates is 35%, while the input parameters are varied as much as 600%. This is also surprising because in many cases the errors seen in clustering appear to be very significant as shown in Figures 4.10 and 4.11. After closer examination it is clear that the increase in clustering errors due to more arrivals is compensated for by an increase in the statistical sample size caused by those additional arrivals. It should be noted that the clustering for these trials is

done very carefully and all by the same person. A different person or a more relaxed approach in using any of these methods can easily result in much higher errors in parameter estimation.

The Fuzzy Weighted Distance Method is recommended as the best method to cluster arrivals for many reasons. As shown by the data in Tables 4.1 - 4.5, the FWDM performs nearly as well or better than both of the other methods for all but two parameter estimates - the σ estimate in Table 4.2 and the Λ estimate in Table 4.3. Also, a visual comparison of cluster assignments confirms the higher accuracy of this method. This approach is also much less dependent on the operator and therefore more repeatable than the RM and the WRM. The FWDM is also by far the fastest of the methods. This is significant issue when large amounts of data need to be clustered.

4.2.2 Measured Performance Prediction Errors

After characterizing the parameter estimate errors, the next step is to examine how the variation in parameter estimates affects performance predictions for MIMO systems. A range of parameter settings are used with a program that generates simulated multipath according to the extended Saleh and Valenzuela model from [2]. At each parameter setting, 1000 data sets are generated and used to calculate the channel matrix for a simple 4 receiver, 4 transmitter MIMO configuration. This is done by assuming that each multipath arrival is a plane wave, and then calculating the signal received at each antenna. Since each arrival comes in at a different direction, the signals will add constructively and destructively based on the antenna position. In this case the 4 antennas at each end are set on the vertical and horizontal axes, $\frac{1}{4}$ wavelength from the origin. The same experiment is then performed on a 10 receiver, 10 transmitter MIMO configuration. Again, the elements are placed every $\frac{1}{4}$ wavelength along the same axes. As the parameters are varied over a $\pm 10\%$ range around a baseline taken from Spencer's parameter estimates ([2]), the mean and standard deviation of the channel matrix elements are evaluated. Varying the parameter results by $\pm 10\%$ shows how a 10% error in the parameter estimate affects the channel

matrix statistics [6]. Along with monitoring the mean and standard deviation of the channel matrix elements, the channel capacity obtained from the water filling solution for each channel matrix is assessed as well. The percentage change in capacity is compared to the percentage change in the parameter values.

A nested loop that varies each parameter ±10% is used to input 32 parameter settings into the multipath generating code. The mean and standard deviation of the channel matrix elements is calculated. Figures 4.12 and 4.13 show histograms of channel matrix elements for two extreme parameter settings. The ±10% variation

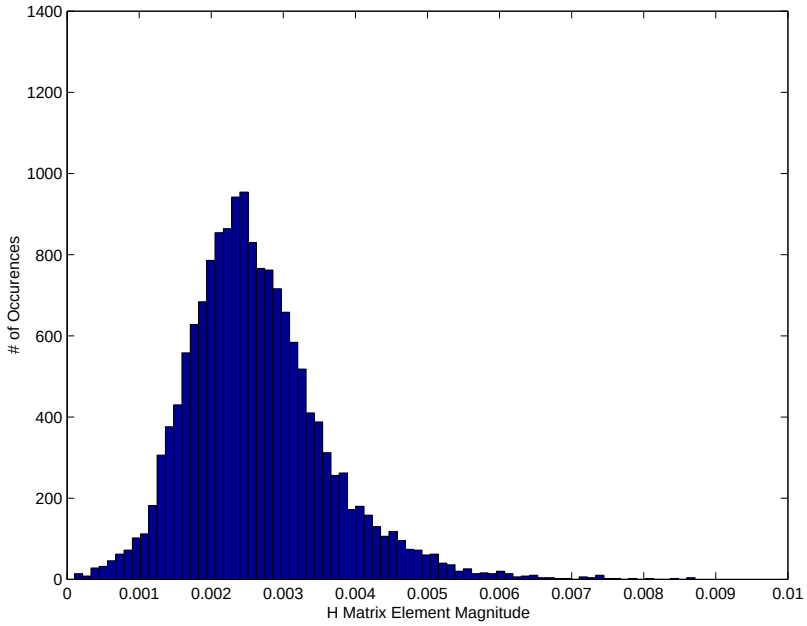

Figure 4.12: All Parameters +10%

in parameter values resulted in ±20% to ± 22% changes in the average signal level for each element. The standard deviation of the signal level at each element varied by ±18% to ± 24%. These large changes in the signal level make sense, since four of the five parameters being swept (all but σ), directly affect the number or amplitude of the multipath arrivals. To measure how the channel matrix element statistical changes

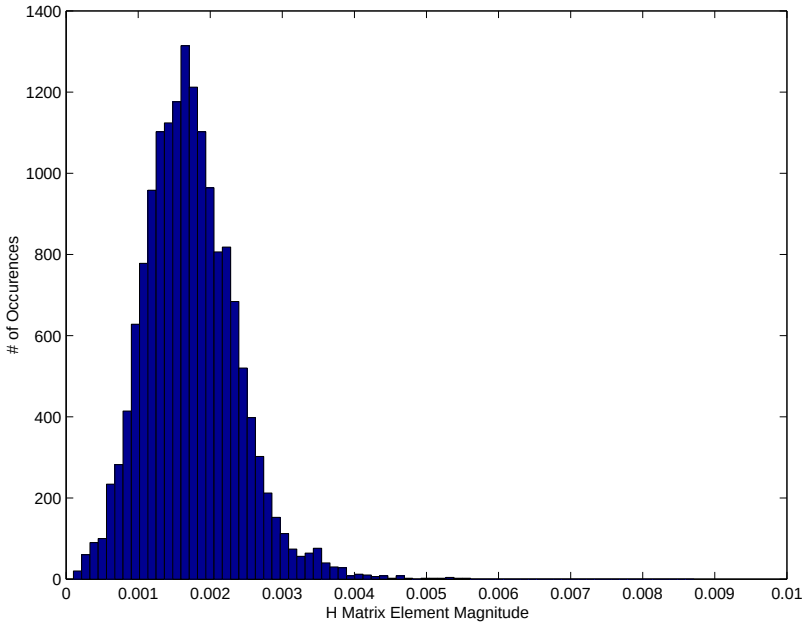

Figure 4.13: All Parameters -10%

affect performance, the capacity of these matrices is calculated. The channel matrix is normalized before computing the capacity so that the capacity variation captured represents changes in the multipath structure and not simply changes in signal power.

Figures 4.14 and 4.15 show the mean and standard deviation of the capacities for each of the 32 parameter sets for the 4 X 4 matrix. The capacity of the 4 X 4 MIMO channel changes $\pm 3\%$, while the parameters are being changed $\pm 10\%$. The standard deviation of the channel capacities changes less than $\pm 7\%$. The capacity changes much less than the channel matrix statistics or the parameters themselves.

Figures 4.16 and 4.17 show the mean and standard deviation of the capacities for each of the same 32 parameter sets for the 10 X 10 matrix. The capacity of the 10 X 10 MIMO channel has more change, at $\pm 7\%$, while the parameters are still being changed $\pm 10\%$. The standard deviation of the channel capacities also changes $\pm 7\%$. The capacity change, while larger than the 4 X 4 case, is still much less than the change in the channel matrix statistics and slightly less than the change in the parameters themselves.

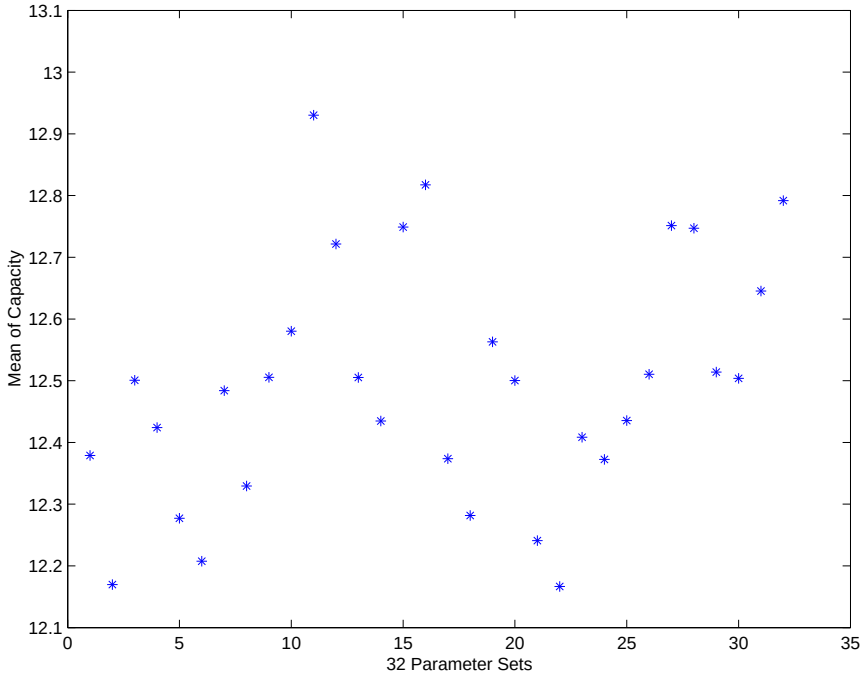

Figure 4.14: Mean of Capacity Estimates for 4 X 4 Matrix

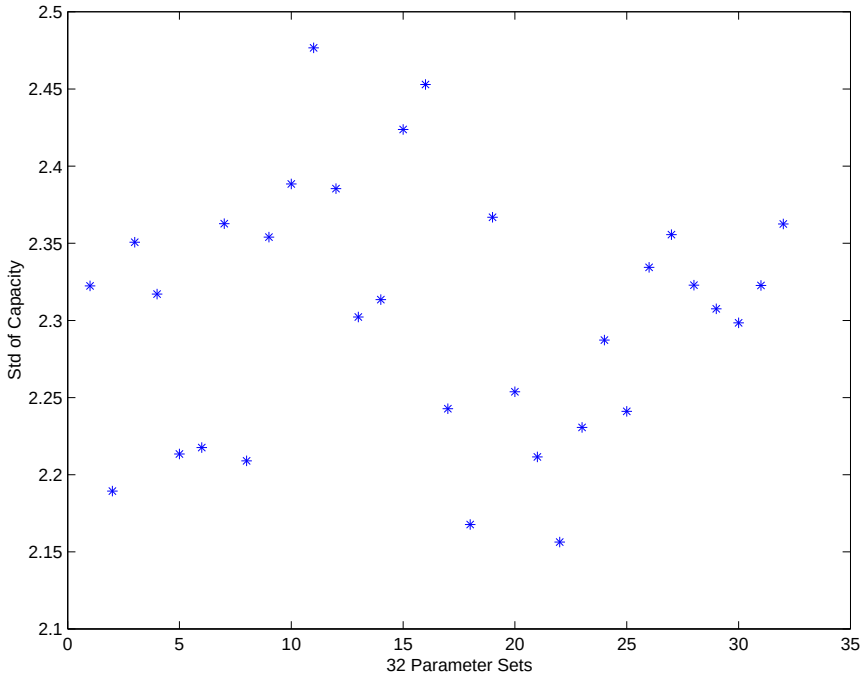

Figure 4.15: Standard Deviation of Capacity Estimates for 4 X 4 Matrix

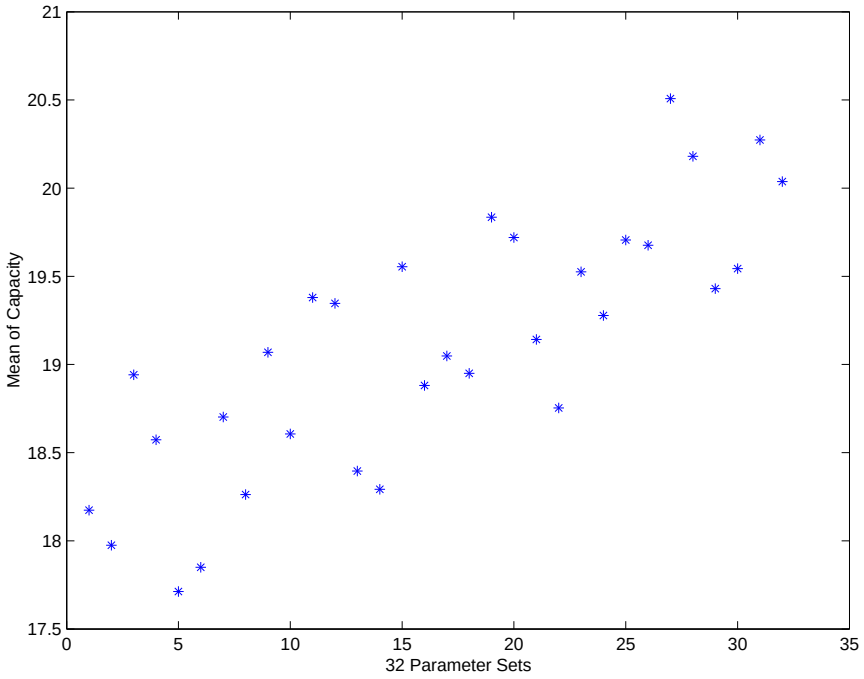

Figure 4.16: Mean of Capacity Estimates for 10 X 10 Matrix

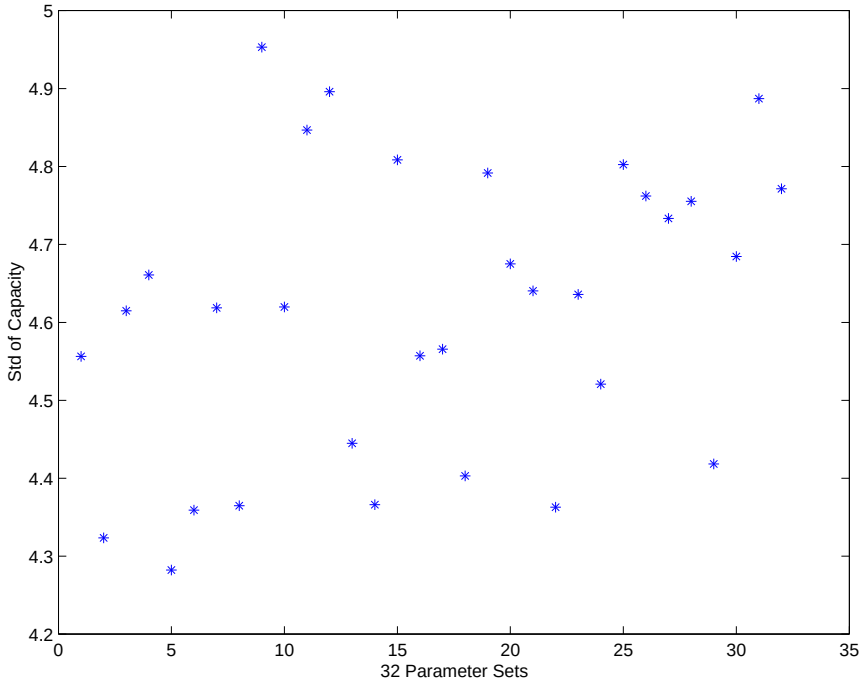

Figure 4.17: Standard Deviation of Capacity Estimates for 10 X 10 Matrix

While these studies seem to indicate that clustering errors do not translate directly to performance prediction errors, it is important to remember a few things. This study was only run for two particular antenna configurations. It is possible that other configurations will show more sensitivity to the variation in parameters. Even if the other confirgurations do not show increased sensitivity to the parameters and to clustering, the clustering process is still important. The purpose of a channel model is to accurately capture and predict as many features of the channel as possible. Even-though one metric for performance indicates that some of the features are irrelevant, other metrics may show otherwise. The closer that a model comes to representing all of the higher order statistics of a channel, the more likely that it will be useful for other configurations. However, based on this experiment, it is concluded that all of these clustering methods produce usable estimates of the model parameters, particularly if capacity is the metric of interest.

The Fuzzy Weighted Distance Method is among the easiest to use, and has slightly superior performance, so it is clearly the best of these methods. However, reviewing the data makes it clear why each of the methods works relatively well. In the cases where the clusters are well isolated and contain relatively few arrivals, the clustering is nearly perfect for all of the methods. In the cases where the clusters overlap, the total number of clusters and arrivals is usually higher. In these cases the larger number of arrivals help to average out the larger number of errors. The end result in each case is usually an acceptable estimate.

Chapter 5

Conclusions

5.1 Contributions

The two systems described in this paper provided valuable information about channel measurement and modeling and the characteristics of indoor wireless communication channels. The 2.4 GHz system showed a drastic increase in multipath arrivals relative to previous channel probing measurements, along with the importance of accurate PSF deconvolution. The 6 GHz system demonstrated the ability to measure the angles of transmission and reception, as well as showing the first step required for characterization of the angle of transmission for multipath returns.

Both systems revealed a multitude of errors that can be made during channel probing as well as during the data processing. While some of the errors in PSF measurements were ignored during the data processing for this work, the steps to avoid or fix those errors were addressed. The need for storing the phase information as well as obtaining repeatable measurements was explained. Many of the problems described in the measurement process were also present, but ignored, in other authors' attempts to probe and characterize channels.

In this thesis several clustering methods were described and their performances were compared. The Fuzzy Weighted Distance Method was presented as the simplest and most effective way to cluster arrivals for parameter estimation. The effects that the errors in the clustering process have on the extended Saleh and Valenzuela model were simulated as well. The most important result of this experiment is the demonstration that the extended Saleh and Valenzuela model is relatively insensitive to

small parameter errors. This reduces the constraints on clustering accuracy and allows more freedom in choosing the minimum number of measurements required for parameter estimation.

5.2 Future Work

As stated above, there are many errors in the system measurements that were not overcome for the systems used. For more accurate channel probing measurements, a system that has less variation from measurement to measurement should be used. The magnitude and phase information of the system PSF and any system measurements should be used for the most accurate and thorough data processing. Antennas that are specifically designed to have nicely shaped antenna patterns at the frequencies of interest as well as having a phase center about which it can be rotated can also improve the quality of measurements as well as simplify the data processing required.

The angle of transmission measurements should be continued to fully characterize the statistics of that parameter, so that the angle of transmission can be added to the Saleh and Valenzuela's model along with the angle of reception. This new model could then be used for complete simulation of MIMO channels using spatially diverse antenna configurations at both the transmit and the receive locations. Work is already being done to directly probe the MIMO characteristics of a channel using multiple antennas in place of the antennas used one at a time for these experiments. As the measurement platforms are improved, the results of the two probing methods should be compared and all differences should be accounted for. This will lend credence to the results of both approaches.

Another very important step for future work is the final validation of the models for use with MIMO antenna configurations. The performance of a MIMO channel should be measured at many locations and then compared statistically to the simulated performance in the same type of environment. This final validation will give much higher confidence to designers desiring to use the model as a performance evaluation tool.

Bibliography

[1] A. A. M. Saleh and R. A. Valenzuela, "A statistical modle for indoor multipath propagation," *IEEE Journal on Selected Areas of Communications*, 1987.

[2] M. A. Jensen Q. H. Spencer, B. D. Jeffs and A. L. Swindlehurst, "Modeling the statistical time and angle of arrival characteristics of an indoor multipath channel," *IEEE Journal on Selected Areas in Communications*, 2000.

[3] J. W. Wallace and M. A. Jensen, "Modeling the indoor mimo wireless channel," *IEE Transactions on Antennas and Propagation*, 2002.

[4] A. L. Swindlehurst J. W. Wallace, M. A. Jensen and B. D. Jeffs, "Experimental characterization of the mimo wireless channel: Data acquisition, analysis, and modeling," *IEEE Transactions on Wireless Communications*, 2002.

[5] J. G. Proakis, *Digital Communications*, McGraw-Hill, 1995.

[6] N. C. Giri, *Multivariate Statistical Analysis*, Marcel Dekker, Inc., 1996.

[7] B. M. Green, "Antenna diversity for personal communications," M.S. thesis, Brigham Young University, 1997.

[8] E. K. Hege, "Psf calibration in astronomical imaging – physical constraints for a noisy problem," *OSA Tech Digest Signal Recovery and Synthesis*, 1998.

[9] J. A. Högbom, "Aperture synthesis with a non-regular distribution of interferometer baselines," *Astronomy and Astrophysics Supplement*, 1974.

[10] D. A. Hawbaker and T. S. Rappaport, "Indoor multipath propagation measurements at 1.3 ghz and 4.0 ghz," *Geoscience and Remote Sensing Symposium*, 1990.

[11] E. Moriyama, M. Mizuno, Y. Nagata, Y. Furuyam, I. Kamiya, and S. Hattori, "2.6 ghz band multipath characteristics for urban microcellular telecommunication systems," *IEEE International Symposium on Personal Indoor and Mobile Radio Communications*, 1991.

[12] D. M. Pozar, *Microwave Engineering*, John Wiley & Sons, 1998.

[13] Q. H. Spencer, "Modeling the statistical time and angle of arrival characteristics of an indoor multipath channel," M.S. thesis, Brigham Young University, 1996.

[14] E. A. Pyper, "Wireless mimo channel probing approach for arbitrary antenna arrays," M.S. thesis, Brigham Young University, 2001.

[15] *MATLAB Function Reference*.

[16] A. K. Jain, *Fundamentals of Digital Image Processing*, Prentice-Hall, 1989.

[17] M. A. Ingram J. H. Jo and N. Jayant, "Angle clustering in indoor space-time channels based on ray tracing," *Vehicular Technology Conference*, 2001.

[18] Y. Oda and T. Taga, "Clustering of local scattered multipath components in urban mobile environments," *Vehicular Technology Conference*, 2002.

[19] J. C. Bezdek, *Pattern Recognition with Fuzzy Objective Function Algorithms*, Plenum Press, 1981.

[20] M. Roubens, "Fuzzy clustering algorithms and their cluster validity," *European Journal of Operational Research*, 1982.

[21] N. R. Pal and J. C. Bezdek, "On cluster validity for the fuzzy c-means model," *IEEE Transactions on Fuzzy Systems*, 1995.

[22] J. W. Wallace and M. A. Jensen, "Characteristics of measured 4x4 and 10x10 mimo wireless channel data at 2.4-ghz," *IEEE Antennas and Propagation Symposium*, 1997.